

# On the creation of high energy bremsstrahlung and intensity by a multitarget and refocusing of the scattered electrons by small-angle backscatter at the wall of a cone and magnetic fields – a possible way to improve linear accelerators in radiotherapy and to verify Heisenberg-Euler scatter

W. Ulmer<sup>1,2</sup>

<sup>1</sup>Klinikum Frankfurt/Oder, Dept. of Radiotherapy, <sup>2</sup>MPI of Biophysical Chemistry, Göttingen, Germany

E-Mail: [waldemar.ulmer@gmx.net](mailto:waldemar.ulmer@gmx.net)

## Abstract

The yield of bremsstrahlung from collisions of fast electrons (energy at least 6 MeV) with a tungsten target can be significantly improved by exploitation of Tungsten wall scatter in a multi-layered target. The Tungsten wall can serve to refocus small angle scattered electrons. It is necessary that the thickness of one Tungsten layer does not exceed 0.02 mm. Further refocusing of electrons results from suitable magnetic fields with field strength between 0.5 Tesla and 6 Tesla (if the cone with multi-layered targets is rather narrow). Linear accelerators in radiation therapy only need refocusing by wall scatter without further magnetic fields (standard case: ca. 100 – 000 plates with 0.01 mm thickness and 1 mm distance between the plates). The construction of a very narrow bremsstrahlung beam with extremely high photon intensity requires an additional strong magnetic field (order 1 – 6 Tesla), which provides the possibility to check Heisenberg-Euler scatter of high energy photons.

## 1. Introduction

A principal problem in the creation of bremsstrahlung of linear accelerators used in radiotherapy and industry/research is the lack of efficiency, since only a rather small part of the created bremsstrahlung is available for further applications. This fact has usually a practical importance with respect to medical accelerators, e.g. in IMRT and stereotaxy, whereas even for a 40 x 40 cm<sup>2</sup> field size at a distance of 100 cm from focus the bremsstrahlung yield is small, and most of it goes lost at the primary collimator and jaws. An additional source of bremsstrahlung loss is the flattening filter, which has to homogenize the transverse profile. As already pointed out, we have usually to deal in radiotherapeutic applications with much smaller field sizes than 40 x 40 cm<sup>2</sup>. Brahme and Svensson (1996) have suggested a linear accelerator using a multiple Beryllium target, and electron energies of the order of 80 – 100 MeV to yield a bremsstrahlung spectrum comparable to a conventional machine with 4 – 6 MeV with a single Tungsten target. However, this concept has the disadvantage that electrons decelerated down to ca. 45 – 50 MeV have to be removed by a magnetic field, since they would produce rather low bremsstrahlung energy in further Beryllium targets.

In this communication, we analyze a multitarget systems consisting of very thin Tungsten layers, i.e. << 0.1 mm to create bremsstrahlung in a much more efficient way by the ordinarily used electron energies between 6 and 20 MeV. However, with respect to industrial/research accelerators this

energetic restriction may not be applicable, and the presented new principle of bremsstrahlung creation also works, if the required photon energy spectrum has to be increased.

This new way of bremsstrahlung creation exploits two physical effects, which can be used for refocusing of scattered electrons, namely the wall scatter of high Z materials such as Tungsten and, as  
5 an additional option, a suitable external magnetic field.

## 2. Material and methods

### 2.1. Schematic representation of bremsstrahlung by a linear accelerator

10 The following figure 1 shows the essential component modules of a linear accelerator. It starts with the impinging electron current on the bremsstrahlung target (usually Tungsten). The foregoing modules of the beam line such as klystron or magnetron, modulator, acceleration tube, deflection of the electron current by bending magnet are not of importance here. Thus in the target two competition processes occur, namely bremsstrahlung creation and multiple scatter of electrons by simultaneous  
15 production of heat.

This multiple scatter and heat production must be regarded as the reason, that the bremsstrahlung creation does not show any preference direction. The beam line according to Figure 1 indicates that only that part of the bremsstrahlung can be used, which can pass through the opening of the primary collimator. The flattening filter immediately below the vacuum window affects the shape of the beam,  
20 which is further controlled by the jaws to obtain the desired field size. However, the flattening filter significantly attenuates the intensity of the photon beam, and due to the inevitable Compton scattering, it also acts as a second source, which affects the shape of the profiles of larger field sizes (e.g. the penumbra).

As a resume we can conclude that the present linear accelerators do not provide a high efficiency, in  
25 particular with regard to the novel irradiation techniques such as Stereotaxy, Rapid Arc, and IMRT, where very small field sizes are required and most of the produced bremsstrahlung goes lost by shielding of the accelerator head (see also Figure 11).

Therefore the question arises, in which way we can significantly improve the yield of bremsstrahlung and reduce the required shielding material in the accelerator head.

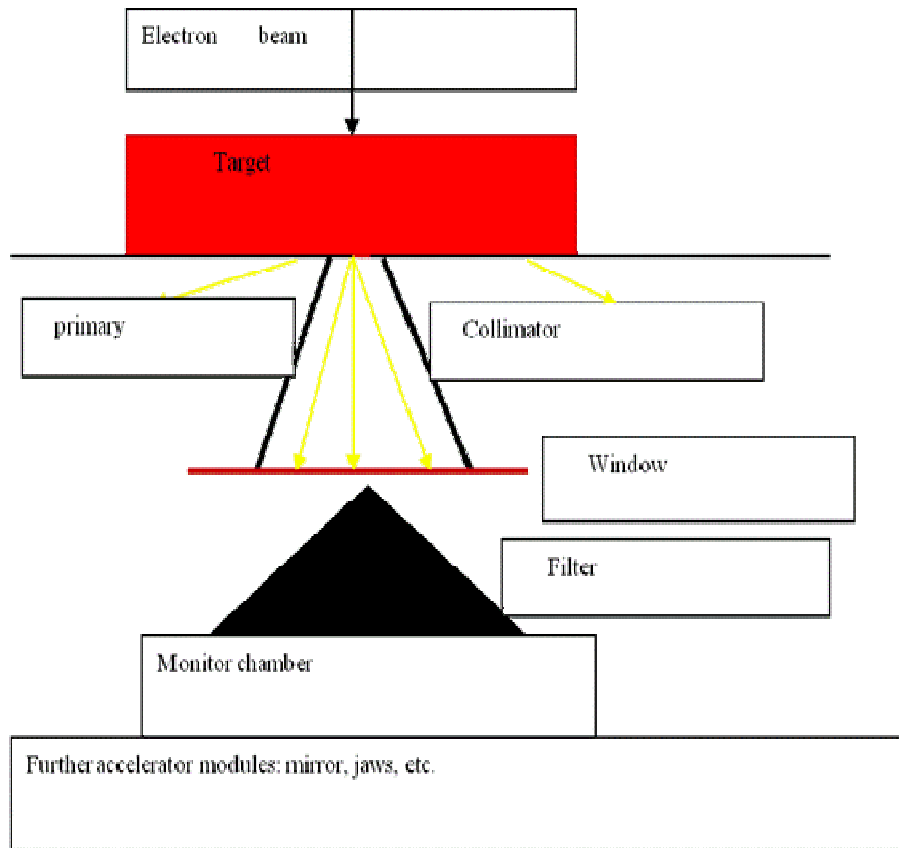


**Figure 1:** Schematic representation of a linear accelerator.

## 2.2. Qualitative considerations with regard to refocusing of electron scatter

Figures 2 and 3 indicate that by restriction to a single Tungsten target there is no mean to prevent the scatter of electrons within the target material.

The thickness of the target of standard linear accelerators amounts to ca. 1 mm Tungsten and immediately below 1 mm Copper in order to increase the removal of the produced heat from the target. The bremsstrahlung spectrum created in Copper is significantly lower than that of Tungsten; it is most widely absorbed in the flattening filter. Since the multiple scatter and heat production are responsible for the low efficiency and for a lot of necessary shielding of the accelerator head, we consider at first an alternative way to exploit bremsstrahlung by a multitarget. This consists of a configuration of very thin Tungsten layers. Their thickness should not exceed 0.02 mm. If we assume a thickness of 0.01 mm for each plate we need 100 plates to reach an overall thickness of 1 mm with an effective depth of 10 cm. Figure 3 qualitatively shows that a tilted wall makes the reflection angle small and therefore the backscatter can be increased. The left-hand side of this figure presents the consequence of this effect, namely a cone configuration of the wall, which embeds ca. 100 Tungsten plates. The heat

production in each plate is negligible and no additional removal of heat is needed. Thus we can verify that the configuration below makes the primary collimator itself to a cone target consisting of ca. 100 plates and the created bremsstrahlung shows the preference direction of a cone. This configuration implies two advantages: The total depth of cone is assumed to amount to 100 mm, and the 100 plates with 1 mm distance between the plates can be regarded as a continuum, i.e., a Tungsten density  $\rho_t$  of the multitarget part of the cone can be assumed. Therefore theoretical calculations can be simplified much. Otherwise, we have to perform complicated numerical step-by-step calculations (this is only possible with regard to Monte-Carlo calculations). The second advantage refers to the direction of the created bremsstrahlung. If the electron energy is much higher than 0.511 MeV (rest energy of the electrons), then the direction of the created bremsstrahlung approximately agrees with the direction of the impinging electrons. Thus bremsstrahlung with large angles cannot be completely avoided, but significantly reduced to a minimum contribution. In a second order, there exists also a refocusing effect of bremsstrahlung at the Tungsten wall due to the small-angle part of the Compton effect.

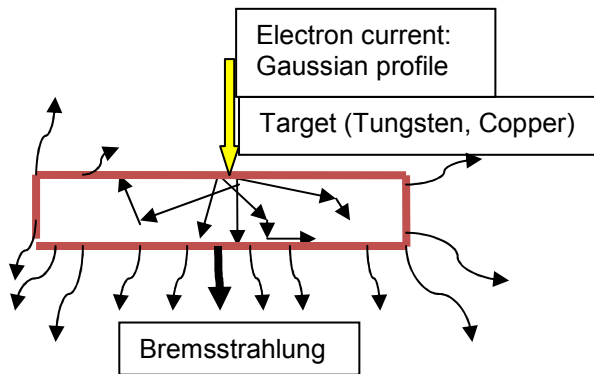


**Figure 2:** Multiple scatter and creation of bremsstrahlung in the target.

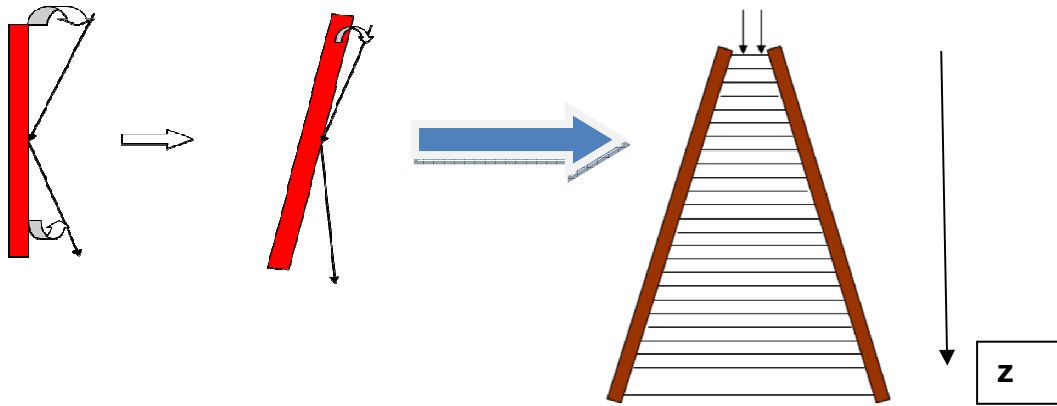


**Figure 3:** Small angle backscatter of electrons at a Tungsten wall (reflection) induces a refocusing of electrons. The backscatter is amplified by a cone configuration of the Tungsten wall.

According to Figure 4 we can exploit and, by that, amplify the refocusing influence obtained by wall scatter, namely by an additional external magnetic field, which must have the property that a permanent gradient of the field component  $B_r$  perpendicular to the propagation axis (z-axis) is present. Thus the complete configuration represents a similarity to features of an electron microscope. The effect of the additional magnetic field is:

1. Reduction of the reflection angle at the Tungsten wall.
2. Reduction of the impinging angle of the inner electrons at each Tungsten plate.

The additional magnetic field makes sense, if the cone is rather narrow, i.e. the opening angle is small and a very narrow radiation beam with extremely high intensity is required. However, the application of an additional magnetic field for refocusing is optional, since many conceptual designs of medical accelerators can already be improved by a configuration without external magnetic field (Figure 3). It should be pointed out that in both Figures 3 and 4 we have used a qualitative presentation based on forestalled results of succeeding sections. The new conceptions of designing linear accelerators can be justified by the following synopsis:

For electrons with energy  $\gg mc^2$  (0.511 MeV) the direction of the created  $\gamma$ -quanta agrees with the actual direction of motion of electrons. This implies for electrons, which suffered large-angle scattering, that the created bremsstrahlung has unfortunately not the preference direction of the incident beam. There is additionally a non-negligible amount of energy loss of electrons and heat production as a consequence of multiple electron scatter.

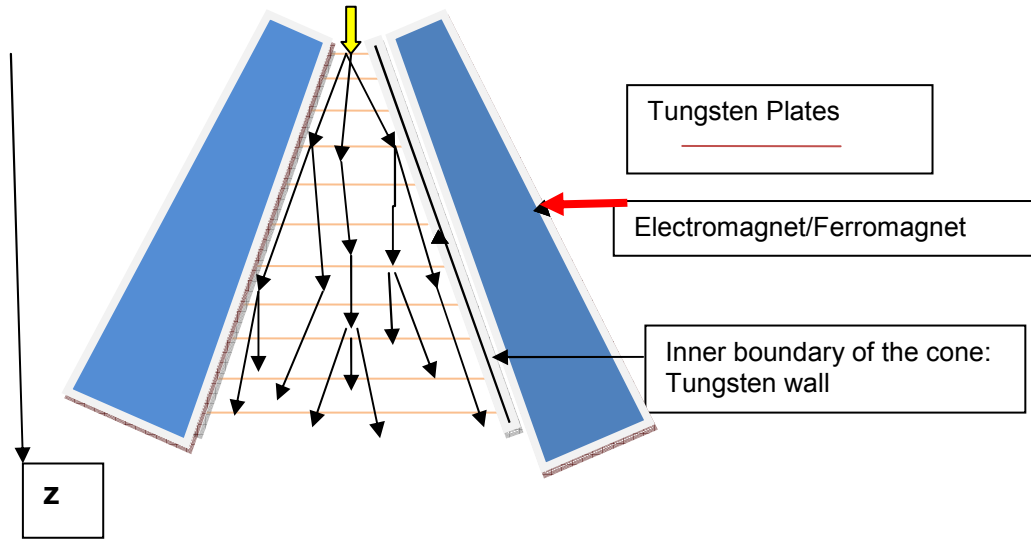


**Figure 4:** Schematic representation of a multi-layered target with an additional magnetic field for refocusing.

A multi-layer target is suitable to reduce multiple scatter significantly by exploiting refocusing effects by the cone wall (high Z material, e.g. Tungsten) and optionally by a proper magnetic field. Thus we have to split the conventional Tungsten target (thickness: usually 1 mm) in, at least, 10 subtargets whose thickness is of the order 0.1 mm and the distance between the layers should then amount to ca. 1 cm. However, a thickness of 0.012 mm (these layers can be purchased) and a distance of ca. 1 - 2 mm between each appears to be much more convenient.

## 2.3. Theoretical calculations and Monte-Carlo calculations with GEANT4

### 2.3.1. Some physical toolkits

#### 2.3.1.1. General properties and requirements

With respect to both calculation procedures (GEANT4 and analytical calculations) we have to use the relativistic energy-momentum relation:

$$W^2 = m^2 c^4 + \vec{p}^2 \cdot c^2 \quad (1)$$

The relativistic energy E of a particle (without rest energy) is given by:

$$\left. \begin{aligned} E &= mc^2 / \sqrt{1 - \beta^2} - mc^2 \\ \beta &= v/c \end{aligned} \right\} \quad (2)$$

The relativistic energy-momentum relation in the presence of a magnetic field (vector potential  $\mathbf{A}$ ) reads:

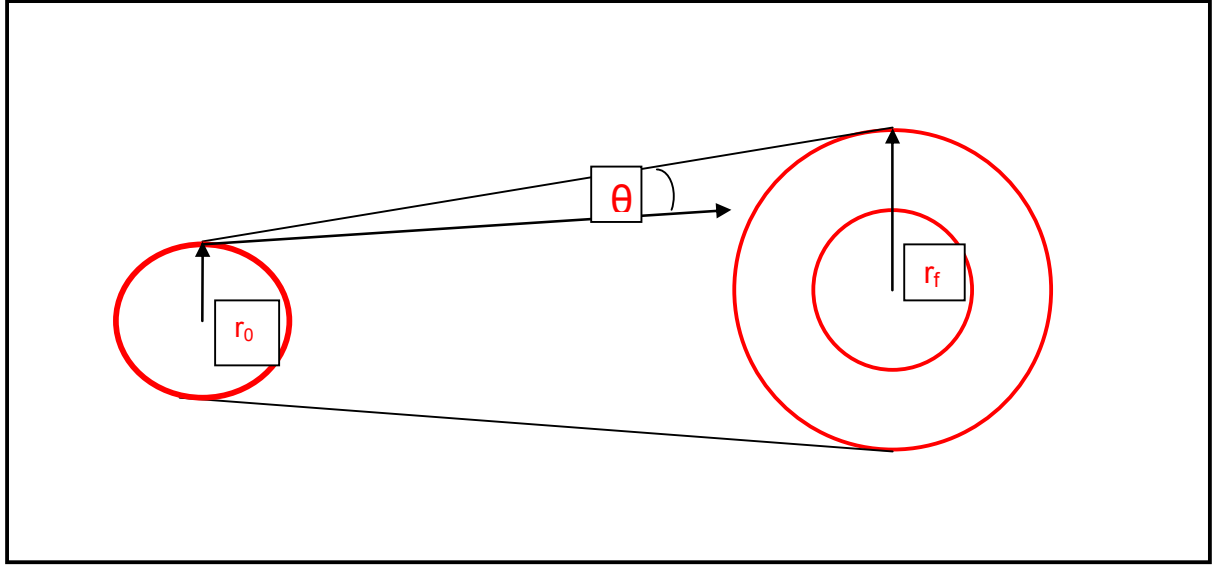
$$W^2 = m^2 c^4 + (\vec{p} - (e/c) \cdot \vec{A})^2 \cdot c^2 \quad (3)$$

Eq. (3) represents a quantum-mechanical equation, if the transition  $\vec{p} \rightarrow \frac{\hbar}{i} \nabla$  is carried out. The

components of the magnetic induction  $\mathbf{B}$  with  $\text{div} \cdot \mathbf{B} = 0$  are given by:

$$\left. \begin{aligned} B_x &= \partial A_y / \partial z - \partial A_z / \partial y \\ B_y &= \partial A_z / \partial x - \partial A_x / \partial z \\ B_z &= \partial A_x / \partial y - \partial A_y / \partial x \\ B_r^2 &= B_x^2 + B_y^2 \end{aligned} \right\} \quad (4)$$

The geometrical configuration is shown in Figure 5.



5 **Figure 5:** Schematic representation of the geometrical properties. On the left-hand side: Small circle of the cone entrance (radius  $r_0$ ) for impinging electron beam. Right-hand side: Larger circle at the cone exit (radius  $r_f$ ). The inner circle symbolizes the area of the entrance. The angle  $\theta$  shows the opening angle of the cone, which is usually small in those cases, where a strong magnetic field is required. This will be verified in the result section.

The field strength has to satisfy, at least, the following properties:

$$\left. \begin{aligned} B_r(z) &= r^2 \cdot B_0 / r_0^2 + (z / L) \cdot (B_f - B_0) \cdot r^2 / r_f^2 \\ r &= r_0 + z \cdot \tan \vartheta = \sqrt{x^2 + y^2} \\ r_f &= r_0 + L \cdot \tan \vartheta \end{aligned} \right\} \quad (5)$$

For the reason of symmetry the following condition has to be valid:

$$|B_x| = |B_y| \quad (6)$$

In the above equation  $B_r(z)$  means the radial component as a function of  $z$ ,  $r_0$  is the field radius at the entrance of the beam ( $z = 0$ ), and  $r_f$  the related radius at the end ( $z = L$ ). With regard to results we mainly deal with lengths  $L = 10$  cm and  $L = 20$  cm of the central axis. The possible devolution of

some cases of interest is shown in Figure 6. However, the properties of this figure do not represent a rigid scheme, since it mainly depends on the design of the target, whether other lengths  $L$  of the cone (central axis) are required. We want also point out that the magnetic field does not disappear at  $z = L$ . This length has only to agree with the focusing part of the magnetic field, whereas a small area with a defocusing part cannot be avoided. It may serve to remove those electrons with sufficiently low energy, where the production of bremsstrahlung is no longer desired.

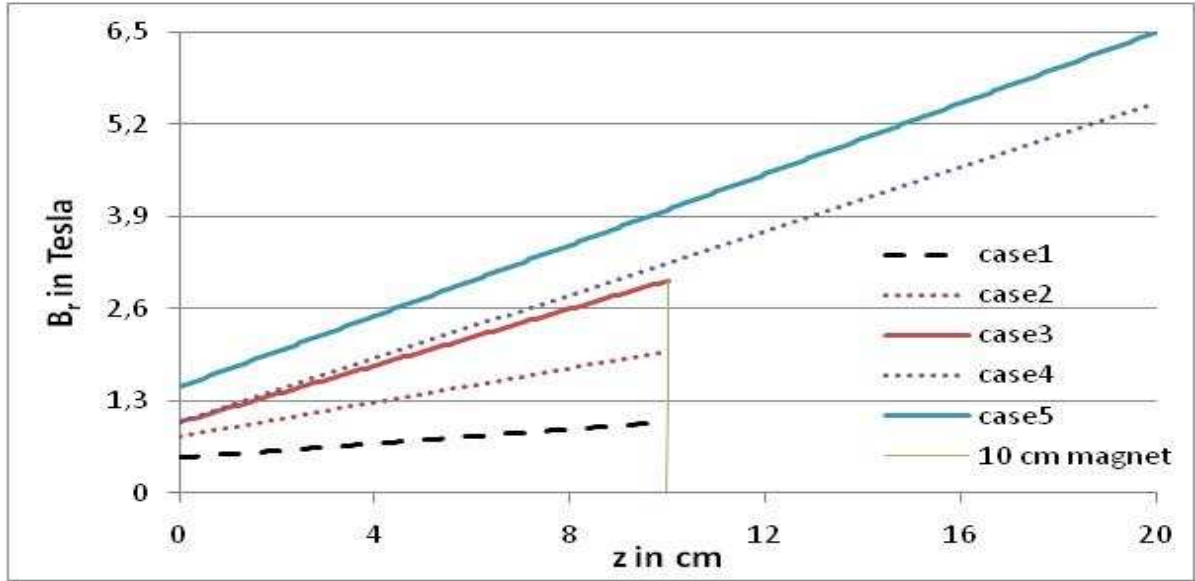


**Figure 6:** Increase of the radial component  $B_r$  along the surface of the cone,  $L$  either 10 cm or 20 cm.  $M_1 =$  case 1:  $B_0 = 0.5$  Tesla,  $B_f = 0.8$  Tesla;  $m_2 =$  case 2:  $B_0 = 1$  Tesla,  $B_f = 2$  Tesla;  $m_3 =$  case 3:  $B_0 = 1$  Tesla,  $B_f = 3$  Tesla;  $m_4 =$  case 4:  $B_0 = 1$  Tesla,  $B_f = 5.5$  Tesla;  $m_5 =$  case 5:  $B_0 = 1.5$  Tesla,  $B_f = 6.5$  Tesla.

A further case  $m_6$  not shown in this figure, but used in calculations, starts with  $B_0 = 2$  Tesla and end in the focusing domain with  $B_f = 7$  Tesla.

### 2.3.1.2. Cross-sections (Dirac equation, Hartree-Fock procedure)

The succeeding formula presents the differential cross-section  $q(\theta)$  of the scattering of fast electrons (relativistic energies) at screened Coulomb potentials of high  $Z$  nuclei. In the nonrelativistic limit and by putting the form factor function  $F(\theta) = 0$  we obtain the Rutherford formula, which shows the awkward property to diverge for small angles  $\theta$ , i.e., if  $\theta \rightarrow 0$  the Rutherford formula and the relativistic extension derived from the Born approximation and Dirac equation lead to unphysical results. As we could verify from the preceding section, the small-angle scatter plays an important role in our considerations. Therefore the form factor function  $F(\theta)$  cannot be ignored.



$$\left. \begin{aligned} q(\vartheta) &= 4 \cdot e^4 \cdot E^2 \cdot [1 - \beta^2 \sin^2(\vartheta/2)] \cdot [Z/Q^2 - F(Q)]^2 \\ Q &= 2 \cdot p \cdot \sin(\vartheta/2) \\ p &: \text{amount of initial momentum} \end{aligned} \right\} \quad (7)$$

A principal problem of all considerations is the determination of the form factor function  $F(\theta)$ , since the evaluation of the scatter formula provides unphysical results for small scatter angles. With regard to Eq. (7) we should point out that the magnitude  $Q$  results from the Fourier transform of the total electron density around a nucleus (Feynman 1962). Therefore we need the electron density  $\rho$  as a function of the nuclear charge  $Z$  for heavy  $Z$  materials such as Tungsten (W:  $Z = 74$ ), Lead (Pb:  $Z = 82$ ) and Tantalum (Ta:  $Z = 73$ ). The best method to determine  $F(\theta)$  is the Hartree-Fock-Dirac method (HFD method). It would also be possible to use the Hartree-Fock method in conjunction with the Schrödinger equation of many electrons in the Coulomb field of a heavy nucleus. However, in view of elastic small angle scatter, where the projectile electrons only 'see' a weakly screened nucleus, the charge density in this domain is important. Due to the high  $Z$  of the considered nuclei relativistic effects in quantum mechanics cannot be neglected. For this purpose we start with the Dirac equation for  $Z$  electrons in the nuclear Coulomb field  $V(r)$ .

$$\left. \begin{aligned} H_{D,j} &= [c \cdot \vec{\alpha} \cdot \vec{p} + \beta \cdot mc^2 + V(r)]_j \\ V(r_j) &= -Ze^2/r_j \\ \vec{p}_j &\Rightarrow \nabla_j \end{aligned} \right\} \quad (8)$$

For a free particle the Pauli principle can be satisfied with one Slater determinant, i.e.

$$\Phi = \frac{1}{\sqrt{N!}} \left| \begin{array}{c} \varphi_1(1) \dots \varphi_1(N) \\ \varphi_2(1) \dots \varphi_2(N) \\ \dots \dots \dots \\ \varphi_N(1) \dots \varphi_N(N) \end{array} \right| \quad (9)$$

Without electron-electron interaction the Slater determinant of Eq. (9) would represent an exact solution of the Dirac Hamiltonian (8), and the Pauli principle is accounted for by this determinant. However, due to electron-electron interactions we have to add a further term to Eq. (8), and we now obtain:

$$H_D = \sum_{j=1}^Z H_{D,j} + \frac{1}{2} \cdot \sum_{j=1}^Z \sum_{k=1, k \neq j}^Z \frac{e^2}{|\vec{r}_j - \vec{r}_k|} \quad (10)$$

With regard to Eq. (9) and Eq. (10) we do not obtain exact solutions. The Hartree-Fock-Dirac method

is a suitable procedure to obtain solutions with sufficient accuracy. We use the following basis set for the evaluation of the HFD procedure:

$$\varphi(x) = \sum_{j=0}^N \left[ A_j \cdot H_j(\alpha_1 \cdot x) \cdot \exp(-\frac{1}{2} \cdot \alpha_1^2 \cdot x^2) + B_j \cdot H_j(\alpha_2 \cdot x) \cdot \exp(-\frac{1}{2} \cdot \alpha_2^2 \cdot x^2) + C_j \cdot H_j(\alpha_3 \cdot x) \cdot \exp(-\frac{1}{2} \cdot \alpha_3^2 \cdot x^2) \right] \quad (11)$$

$$\left. \begin{aligned} \varphi(x, y, z) &= \varphi(x) \cdot \varphi(y) \cdot \varphi(z); \\ N &= Z/2 \quad (N : \text{even}); \quad N = (Z+1)/2 \quad (N : \text{odd}) \end{aligned} \right\} \quad (11a)$$

- 5 The Slater determinant has to account for an open shell case, if  $Z$  is odd. The parameters  $\alpha_1, \alpha_2, \alpha_3$  refer to trial functions and have been determined by energy minimization:

$$\left. \begin{aligned} \alpha_1 &= 1.27 \cdot 10^{-7} / Z \\ \alpha_2 &= 0.96 \cdot 10^{-7} / \sqrt[3]{Z} \\ \alpha_3 &= 0.51 \cdot 10^{-7} \end{aligned} \right\} \quad (12)$$

For computational reasons, i.e., the evaluation of all necessary integrals of HFD, it is useful to write the basis set Eq. (11) in a modified form in order to evaluate all integrals containing Coulomb

- 10 interactions in a convenient way:

$$\left. \begin{aligned} \varphi(x) &= \sum_{j=0}^N \left\{ [A'_j \cdot x^j \cdot \exp(-\frac{1}{2} \cdot \alpha_1^2 \cdot x^2) + B'_j \cdot x^j \cdot \exp(-\frac{1}{2} \cdot \alpha_2^2 \cdot x^2) + C'_j \cdot x^j \cdot \exp(-\frac{1}{2} \cdot \alpha_3^2 \cdot x^2)] \right\} \\ \varphi(x, y, z) &= \varphi(x) \cdot \varphi(y) \cdot \varphi(z) \end{aligned} \right\} \quad (13)$$

The evaluation of Eq. (9) together with Eq. (10) and Eq. (13) is, in the meantime, a standard procedure. The Slater determinant can be computed with ease and can be expected on shell case, if  $Z$  is odd.

$$\left. \begin{aligned} \delta E = 0 &\rightarrow \delta \int \Phi^* H \Phi d^3 x_1 \dots d^3 x_Z = 0 \\ \int \Phi^* \cdot \Phi d^3 x_1 \dots d^3 x_Z &= 1 \end{aligned} \right\} \quad (14)$$

15

In our problem, we are mainly interested in the knowledge of the electron density  $|\Phi^* \cdot \Phi|^2$  of some high  $Z$  materials like Pb, Ta and W with regard to the accurate calculation of the form factor function  $F(\theta)$  according to Eq.(7). HFD calculations have been performed by many authors (Aerts et al 1985, Aerts 1986, Quiney et al 1989, Visser et al 1992, Grant et al 2002). In particular, Salvat et al (1987) have

20 calculated shielding factors of similar problems. However, they only used radial solutions, and spin-orbit couplings have been neglected.

### 2.3.1.3. Magnetic lenses

At first, we have to point out that our problem, namely the refocusing of scattered electrons by plates with high  $Z$  material with the help of a magnetic field, in a certain sense resembles an electron microscope. The usual magnetic lenses system in electronic microscopes allows partially a nonrelativistic approach, since only electron energies of about 200 – 300 keV are required. We should point out that it would be possible to focus even the higher energetic electrons by low magnetic fields, but this would imply long distances for the focusing planes.

The resonance frequency (Eq. (15)) now reads ( $B$ : magnetic induction,  $B = B_0$  for constant magnetic fields,  $E$ : relativistic kinetic electron energy):

$$\omega = (e/m) B_0 \cdot \sqrt{1 - u^2/c^2} \quad (15)$$

Eq. (15) is only valid for  $B = B_0$ . In the inhomogeneous case, one has to choose the position with the maximum field strength and to correct the Larmor frequency  $\omega$  by the perturbation influence due to the environment. In general,  $\omega$  is a function of the coordinates. The so-called orbit-equation for the relativistic particle moving in a magnetic field now becomes:

$$d^2 r / ds^2 \cdot u^2 / \sqrt{1 - u^2/c^2} = -\frac{1}{4} e / [m^2 (1 - u^2/c^2)] B^2 r \quad (16)$$

The reciprocal focus length  $1/f$  is given by:

$$1/f = \frac{1}{8} \frac{e^2}{E^2} \int B^2 dz \quad (17)$$

The distance between two orbits is calculated by the following equation, where the parameters have to be accounted for:

$$\cos(\varphi) : \text{angle between } u(z\text{-axis}) \text{ and transversal component}(x/y)$$

The velocity  $u$  in direction to  $z$ -axis refers to the motion of the impinging electrons, i.e. the state without scatter, the  $x/y$  component refers to the average value due to scatter in a subtarget.

$$\left. \begin{aligned} L_s &= \frac{2\pi \cos(\varphi)}{(e/m)B} \\ u &= c \sqrt{E^2 + 2Emc^2} / (E + mc^2) \end{aligned} \right\} \quad (18)$$

However, formula (18) referring to  $u$  has to be used for both components of the electron motion, if the scattered electrons can also travel in the  $x/y$ -plane with relativistic energies.

Since the description of the scattering of electrons in the target material leads to a Gaussian kernel

with an increasing  $\sigma(z)$ , the deconvolution of this Gaussian, worked out in other papers and discussed and forthcoming section, is used for the determination of the local field strength  $B(x, y, z)$ . The principle of a magnetic lense mainly serves as a guide in our study, since we have to consider an extended Tungsten cone as the 'object' of the lense, whereas the created bremsstrahlung can be used for imaging.

### 2.3.2. Fermi-Eyges theory, multiple scatter theory of Molière and inclusion of magnetic fields

Fick's law of diffusion plays a key role in a lot of physical/chemical/physiological processes, it is also used for the description of scatter and absorption of electrons, protons or neutrons in a medium such as Tungsten, and it may now be referred to as Fermi-Eyges age equation (Eyges 1948).

$$-\frac{\partial}{\partial t} \rho + D \Delta \rho = 0 \quad (19)$$

With respect to Fick's law  $D$  is the diffusion coefficient,  $\rho$  the particle (electron) density (concentration) and  $\Delta$  the Laplace operator. In the case of the Fermi-Eyges theory, the particle density  $\rho$  has to be replaced by an energy-distribution density  $E$ , which reads:

$$-\frac{\partial}{\partial t} E + D_F \Delta E = 0 \quad (20)$$

Since both equations formally agree, we now introduce the amplitude  $U$  in order to be independent of the actual meaning. The same fact is also valid with regard to the constant factor  $D$ , which may either be identified with a diffusion constant  $D$  or with a parameter  $D_F$  in Fermi-Eyges theory. Eqs. (19 - 20) follow from the property that a gradient of the density is connected with a current:

$$\mathbf{j} = -D \cdot \nabla U \quad (21)$$

In addition, a balance equation has also to hold:

$$\left. \begin{aligned} \frac{\partial}{\partial t} U + \text{div} \mathbf{j} &= 0 \\ \text{div} \mathbf{j} &= (\nabla \cdot \mathbf{v}) U \end{aligned} \right\} \quad (22)$$

The term  $\nabla \cdot \mathbf{v}$  represents the scalar product of the 3D differential operator  $\nabla$  with a 3D velocity  $\mathbf{v}$ . If the particles have the charge  $q$  (for electrons:  $q = e$ ) and a magnetic field, described by the vector potential  $\mathbf{A}$ , is present, then an additional momentum/velocity due to the magnetic field

(Lorentz force) has to be accounted for:

$$\left. \begin{aligned} \mathbf{p} &= -\frac{e}{c} \mathbf{A} \\ \mathbf{v} &= \mathbf{p} / m = -\frac{e}{c m} \mathbf{A} \\ \text{div} \mathbf{A} &= \nabla \cdot \mathbf{A} = 0 \end{aligned} \right\} \quad (23)$$

5 The velocity  $\mathbf{v}$  results from the division of the momentum  $\mathbf{p}$  by the particle mass  $M$  (= electron mass  $m$ ) and  $c$  is the velocity of light. Now Eq. (21) and the continuity Eq. (22) read:

$$\left. \begin{aligned} \mathbf{j} &= -\left(\mathbf{D} \cdot \nabla - \frac{e}{mc} \mathbf{A}\right) \mathbf{U} \\ \frac{\partial}{\partial t} \mathbf{U} + \text{div} \mathbf{j} &= 0 \\ -\frac{\partial}{\partial t} \mathbf{U} + \mathbf{D} \cdot \Delta \mathbf{U} - \frac{e}{mc} (\mathbf{A} \cdot \nabla) \mathbf{U} &= 0 \end{aligned} \right\} \quad (24)$$

The last equation can also be written in the form

$$10 \quad -\frac{\partial}{\partial t} \mathbf{U} + \mathbf{D} \cdot \Delta \mathbf{U} - \text{div} (\mathbf{v} \mathbf{U}) = 0 \quad (25)$$

If we replace  $\mathbf{U}$  by a probability distribution  $P$ , then Eq. (25) turns out to be the Kolmogorov forward equation, and we regard  $\mathbf{v}$  as an effect of a magnetic field. However, equations (24 -25) are not yet fully gauge invariant, since we have only modified the diffusion current  $\mathbf{j}$  by the magnetic interaction. The magnetic effect is not yet included in the balance equation. In order to complete this condition we have to write:

$$\left. \begin{aligned} \frac{\partial}{\partial t} \mathbf{U} + \left(\nabla - \frac{e}{mcD} \mathbf{A}\right) (\mathbf{D} \cdot \nabla - \frac{e}{mc} \mathbf{A}) \mathbf{U} &= 0 \\ -\frac{\partial}{\partial t} \mathbf{U} + \mathbf{D} \cdot \Delta \mathbf{U} - \frac{2e}{mc} (\mathbf{A} \cdot \nabla) \mathbf{U} + (e^2 \mathbf{A}^2 / D m^2 c^2) \mathbf{U} &= 0 \end{aligned} \right\} \quad (26)$$

20 Besides gauge invariance a further reason for obtaining Eq. (26) is the transition to the Schrödinger equation with magnetic field, since the simple Fick's law of diffusion can be transformed to a Schrödinger equation without external fields. Eq. (26) provides a correspondence in the presence of an external magnetic field. It should be noted that the Kolmogorov forward equation is contained as in the special case of Eq. (26) by setting  $\mathbf{A}^2 = 0$ . According to the Fermi-

Eyges/diffusion theory we can always put

$$\sigma^2 = 2Dt \text{ or } \sigma^2 = 2D\tau \quad (26a)$$

5 The parameter  $\tau$  can replace the arbitrary time-variable  $t$ , if scatter/diffusion only occurs in a short time interval. We consider the case, where the  $z$ -component  $B = B_z = B_0$  of a constant magnetic field is responsible for the motion of electrons and pass to the general case thereafter. Since the magnetic field strength  $B_0$  is given by  $B = \text{rot } A = \nabla \times A$ , we can choose  $A$  as follows:

$$\left. \begin{aligned} A_x &= -By/2, \quad A_y = Bx/2 \\ B_z &= \partial A_y / \partial x - \partial A_x / \partial y = B_0 \\ A^2 &= B_0^2 (x^2 + y^2) / 4 \end{aligned} \right\} \quad (27)$$

10 By that, Eq. (27) becomes ( $U = E$ ):

$$\left. \begin{aligned} -\partial E / \partial t + D_F \Delta E + (e^2 B_0^2 / 4 m^2 c^2 D_F)(x^2 + y^2)E \\ - (eB / cm)[y\partial / \partial x - x\partial / \partial y]E = \lambda_1 E \end{aligned} \right\} \quad (28)$$

Since in  $z$ -direction motion without magnetic interaction is allowed, the following separation of the above equation is possible:

$$E = \varphi(x, y, t) \exp(-\lambda_1 t) \exp(ikz) \exp(-k^2 D_F t) \quad (29)$$

15

This provides the following equation:

$$\left. \begin{aligned} (\partial^2 / \partial x^2 + \partial^2 / \partial y^2) \varphi - (\omega_0 / D_F)[y\partial / \partial x - x\partial / \partial y] \varphi \\ + (\omega_0^2 / 4 D_F^2)(x^2 + y^2) \varphi = (1 / D_F) \partial \varphi / \partial t \end{aligned} \right\} \quad (30)$$

The following parameters are given by:

$$\begin{aligned} \omega_0 &= eB_0 / mc \quad (31) \\ \lambda &= \lambda_1 + \lambda' \quad (31a) \end{aligned}$$

20

It has to be pointed out that the Larmor frequency  $\omega_0$  according to Eq. (31) is identical with those obtained by a Schrödinger or Dirac equation with an external magnetic field. The basis solution (generating function) from which we can construct all other solutions (see e.g. comparison with  
25 Schrödinger equation) is given by

$$\varphi(x, y, t) = \exp[-a(x^2 + y^2)/2] \exp(-\lambda' t) \quad (32)$$

$$\lambda' = \pm i \omega_0 \quad (33)$$

$$a^2 = -\omega_0^2 / 4 D_F^2 \Rightarrow a = \pm i \omega_0 / 2 D_F \quad (33 a)$$

The parameters  $a$  and  $\lambda'$  represent complex values; however, we can form a linear combination to get the real solution: Before we shall consider this property, we note that with respect to the z-coordinate a set of solutions of the diffusion equation are permitted (see Ulmer 1983). They result from the Fourier transform of the specified z-dependent function:

$$\Phi(z, t) = \frac{1}{\sqrt{2\pi}} \int_{-\infty}^{\infty} A(k) \exp(ikz) \exp(-k^2 D_F t) dk \quad (34)$$

$$A(k) = a_0 + a_1 k + a_2 k^2 + \dots + a_n k^n$$

Every power of  $k$  of the expansion of  $A(k)$  represents a solution, if the integral is carried out. We therefore denote

$$\Phi_n(z, t) = P_n(z, t) \exp(-z^2 / 4 D_F t) \quad (35)$$

The polynomials  $P_n(z, t)$  have been previously defined by evaluation of the above integral (34):

$$\Phi(z, t) = \frac{1}{\sqrt{2\pi}} \int_{-k_0}^{k_0} \exp(ikz) \exp(-D k^2 t) dk / 2k_0 \quad (36)$$

The boundary parameter  $k_0$  is given by  $k_0 = 1/z_0$ . The evaluation of the integral (29) provides

$$\left. \begin{aligned} \Phi(z, t) &= U(t) \exp(-z^2 / 4 D_F t) [\operatorname{erf}(s_1) - \operatorname{erf}(s_2)] \\ U(t) &= z_0 / 4 \sqrt{2 D_F t} \\ s_1 &= (1/z_0 + iz / 2 D_F t) / \sqrt{D_F t} \\ s_2 &= (-1/z_0 + iz / 2 D_F t) / \sqrt{D_F t} \end{aligned} \right\} \quad (37)$$

With the help of Eq. (37) we consider the solution:

$$\left. \begin{aligned} E(x, y, z, t) &= \Phi(z, t) \cdot \exp(-\lambda_1 t) \varphi \\ \varphi &= A_0 \cos(\omega_0 (x^2 + y^2) / 4 D + \omega_0 t) + A_1 \sin(\omega_0 (x^2 + y^2) / 4 D_F + \omega_0 t) \end{aligned} \right\} \quad (38)$$

The sine and cosine function appears by forming linear combinations of solutions of Eq. (32), since according to Eq. (34) is an imaginary parameter and the theorem for complex exponential functions can be applied. It has to be mentioned that the cosine as well as the sine are solutions, and both may form linear combinations according to Eq. (37). We should account for that the function  $\varphi$  in Eq. (28) has not to be restricted to the simple sine and cosine, but we can also use

the general solution manifold according to Eqs. (37 - 38).

Before we shall study some properties of Eq. (38), a comparison with the Schrödinger equation is indicated.

The free particle Schrödinger equation is given by

$$5 \quad i\hbar \partial \Psi / \partial t = - (\hbar^2 / 2m) \Delta \Psi \quad (39)$$

It assumes the character of an irreversible transport equation, if the substitution  $t = i\tau$  is carried out. By that, the diffusion constant is given in terms of the Planck's constant:  $D_F = \hbar / 2m$ .

However, the solution (38) is not the only possible one, and we are able to obtain a spectrum of solutions and their linear combination. Thus the following solution can also be satisfied:

$$10 \quad \left. \begin{aligned} \varphi &= A_0 \cos^2((\omega_2 / 4D_F)(x^2 + y^2) + \omega_2 t) - A_1 / 2 \\ \omega_2 &= \omega_0 \cdot 2 \end{aligned} \right\} \quad (40)$$

The complete solution spectrum is given by the two different types:

Powers of even order:

$$\left. \begin{aligned} \varphi_{2n} &= \sum_{m=0}^n \left\{ A_{2m} \cos^{2m}((\omega_{2n} / 4D_F)(x^2 + y^2) + \omega_{2n} t) \right. \\ &\quad + \left. B_{2m} \sin^{2m}((\omega_{2n} / 4D_F)(x^2 + y^2) + \omega_{2n} t) \right\} \\ \omega_{2n} &= \omega_0 \cdot 2n \quad (n \geq 1, n = 1, 2, 3, ) \end{aligned} \right\} \quad (41)$$

Powers of odd order:

$$15 \quad \left. \begin{aligned} \varphi_{2n+1} &= \sum_{m=0}^n \left\{ A_{2m+1} \cos^{2m+1}((\omega_{2n+1} / 4D_F)(x^2 + y^2) + \omega_{2n+1} t) \right. \\ &\quad + \left. B_{2m+1} \sin^{2m+1}((\omega_{2n+1} / 4D_F)(x^2 + y^2) + \omega_{2n+1} t) \right\} \\ \omega_{2n+1} &= \omega_0 \cdot (2n+1) \quad (n \geq 0, n = 0, 1, 2, 3, ) \end{aligned} \right\} \quad (42)$$

Please note that superpositions of different order and related eigen-frequencies are also possible solutions. Thus we can perform a linear combination of all solutions, e.g. a fast oscillating solution with a slow oscillating solution can be combined to form beat oscillations.

At first, we look at the connection between diffusion and the quantum mechanical Schrödinger equation with external magnetic fields. The following aspects should be emphasized: The



resonance conditions for  $\omega_0$  are in both cases identical, this appears to be rather noteworthy. In a formal sense, we have only to substitute the real time  $t$  by an imaginary time  $\tau \Rightarrow it$ , and the reversibility of the Schrödinger equation goes lost. This behavior is also known from the path integral formulation according to Feynman (Feynman and Hibbs 1965), which represents a further possible way to solve the complicated task of scatter and the role of magnetic fields by perturbation theory.

With respect to the eigenfrequency  $\omega_0$  and its dependence on the related parameters  $e$ ,  $m$  and  $B$  we are able to make the following statements:

The z-part of the solution has also the character of an oscillator due to the complex argument yielding nodes (see e.g. the book of Abramowitz and Stegun 1970). Only for sufficient large time  $t \Rightarrow \infty$  a homogeneous charge distribution will be reached. The x – y – part does not allow broadening by diffusion. The behavior is comparable to that of a magnetic lense. Let us now consider an example of a magnetic bifurcation. Assume an oscillating propagation in the x-y plane with the highest frequency  $\omega_0$  given by the magnetic field strength  $B_0$ . Thus a sudden change of the magnetic field strength from  $+B_0$  to  $B_0' = B_0 + \Delta B_0$  leads to a magnetic bifurcation, and, in particular, the antisymmetric sine functions change the sign, when the argument becomes negative. Such an effect may be induced by an inhomogeneous magnetic field yielding changes of the field strength (amount and orientation). The symmetry is spontaneously broken. The same fact may also happen under a lot of similar external influences: The change of the homogeneity of the magnetic field yields a change of the diffusion constant  $D_F$ ; a change of the energy distribution  $E$  may require the formation of complete different patterns and oscillation frequencies, etc.

A principal result of the Bethe-Heitler theory is that the energy loss due to creation of bremsstrahlung is proportional to the actual electron energy. The differential equation for the radiation loss reads (in one dimension):

$$-dE_{bre}/dz = X_{rl}^{-1} \cdot E_{bre} \quad (43)$$

The theory of the creation of ‘bremsstrahlung’ can be formulated by the propagator method (Feynman 1962). With regard to cross-sections  $q_{br}$  for bremsstrahlung the corresponding expressions are rather similar as those for  $q(\theta)$  according to Eq. (7). The main difference is that the parameter  $Q$  is different, since for the emission of  $\gamma$ -quanta the energy differences of virtual orbitals have to be accounted for. The above mentioned phenomenological description summarizes all these parameters resulting from the quantum theoretical treatment by the radiation length  $X_{rl}$

according to Eq. (43).

By iteration of Eq. (43) we obtain a second order differential equation, and the extension to 3D can readily carried out, i.e. the Laplace operator  $\Delta$  appears. This extension has the advantage that the resulting equation can be added to further phenomenological equations containing the Laplace operator:

$$-\Delta E_{bre} = X_{rl}^{-2} \cdot E_{bre} \quad (43a)$$

A further advantage results from the previous Figure 3: If the amount of Tungsten sublayers is high, and, by that, the distance between them is small (e.g. 1 mm in the cone target), it is possible to solve Eq. (45a) under continuum conditions. The total Tungsten mass can be divided by the cone volume to obtain the medium density  $\rho_t$ . Step-by-step calculations (we do not report them here) showed that for 2 mm distances between the plates and identical overall mass a continuum approximation can be justified.

In a phenomenological theory, we can summarize the complete problem by including both, energy loss by radiation loss (Bethe-Heitler theory) and energy dissipation (Fermi-Eyges theory)

$$\left. \begin{aligned} -\partial E / \partial t = D_F \cdot \Delta E - (2e/mc) \cdot (\vec{A} \cdot \nabla) \cdot E + \\ (e^2 \vec{A}^2 / D_F m^2 c^2) E + \\ \Delta E_{bre} + \Delta E_{col} = X_{rl}^{-2} \cdot E_{bre} + X_{col}^{-2} \cdot E_{col} \end{aligned} \right\} \quad (44)$$

In Eq. (44) the parameter  $X_{rl}$  is referred to as the radiation length, which is proportional to  $Z^2$ ,  $N_A$  and  $A_N$ , whereas  $X_{col}$  refers to the energy absorption by the cone wall (collimator), which is proportional to  $Z$ ,  $N_A$  and  $A_N$ . The nuclear charge is denoted by  $Z$ , the nuclear mass number by  $A_N$ , and  $N_A$  is the Avogadro number.

The influence of the magnetic field can be accounted by the following solution expansion:

$$\left. \begin{aligned} E(x, y) = \sum_{n=0}^N \{ A_{2n} \cos((\omega_{2n} / 4D_F) \cdot r^2) + \omega_{2n} \tau + B_{2n+1} \cos((\omega_{2n+1} / 4D_F) \cdot r^2) + \omega_{2n+1} \tau \} \\ \omega_n = n e B' / mc = n e (B_0 + \Delta B_0) \quad (Larmor \ frequency) \end{aligned} \right\} \quad (45)$$

$B'$  refers to as a correction of  $B_0$  by  $\Delta B_0$ , since the magnetic induction must not be constant in the volume under consideration. In principle, we have to account for  $N \rightarrow \infty$ , which is impossible in numerical calculations.

There are two possible procedures, which we have worked out:

- **Solution of the scatter problem by a proper magnetic field acting between the subtargets and determination of the corresponding phase space for Monte-Carlo calculations (GEANT4) with respect to collision interaction (Bethe-Bloch) and bremsstrahlung (Bethe-Heitler theory).**
- **Complete solution of the above differential equation containing all 3 components using the tools given by deconvolution and inclusion of magnetic fields. In such a situation we have to put:  $E_{bre} = E_{col} = E$ .**

### 2.3.3. Deconvolution problem of the theory (creation of bremsstrahlung, scatter and refocusing by an external magnetic field)

The scatter as pointed out is described by one Gaussian (diffusion according to Fick's law, energy/fluence broadening by collisions, etc.). Then the origin function refers to a less perturbed situation as it is true for the initial fluence of electrons or  $\gamma$ -rays. With regard to diffusion/heat equation the inverse problem has been studied by Saitoh (2004). The approximation of multiple scatter (Bethe 1953, Molière 1955) by one single Gaussian kernel has been thoroughly described by Svensson and Brahme (1996). The following chapter uses some results presented in previous publications (Ulmer 2010, Ulmer and Matsinos 2010).

We denote the energy/particle fluence of the origin (source) with  $\Phi$ , and the resulting fluence due to scatter with  $\varphi$ . Then the connection between  $\Phi$  and  $\varphi$  may be given by the 2D-Gaussian convolution:

$$\varphi(x, y) = \frac{1}{s^2 \pi} \int \int \Phi(u, v) \cdot \exp[-((x - u)^2 + (y - v)^2) / s^2] du dv \quad (46)$$

The half-width value  $s$  may itself depend on  $z$ , i.e.  $s = s(z)$ , if the convolution is regarded at different planes. Then  $s(z)$  may be related to a projection angle. However, we shall verify that the dependence  $s = s(x, y, z)$  is also possible with regard to Eq. (46) and the forthcoming Eq. (47), which is useful, if magnetic fields are accounted for. The inverse problem, namely the calculation of  $\Phi(x, y)$  from a given function  $\varphi(s, x, y)$ , is carried out by a deconvolution with the inverse kernel  $K^{-1}(s, u-x, v-y)$  and reads:

$$\Phi(x, y) = \int \int K^{-1}(s, u - x, v - y) \cdot \varphi(s, u, v) du dv \quad (47)$$

The inverse kernel  $K^{-1}$  of a Gaussian kernel  $K$  is given by (Ulmer 2010):

$$\left. \begin{aligned} K^{-1}(s, u-x, v-y) &= \sum_{l=0}^{\infty} \sum_{n=0}^{\infty} (-1)^l s^{2l} / (2^l \cdot l!) (-1)^n s^{2n} / (2^n \cdot n!) H_{2l}(s, u-x) H_{2n}(s, v-y) K \\ K &= \frac{1}{s^2 \pi} \exp[-((u-x)^2 + (v-y)^2) / s^2] \end{aligned} \right\} \quad (48)$$

$H_{2n}(s, u-x)$  are Hermite polynomials of even order. The above formulas are also valid for the so-called composite kernels, i.e.  $s_1$  and  $s_2$  refer to Gaussian kernels. The resulting convolution obtained after convolution with first  $s_1$  and second with  $s_2$  is identical to one convolution carried out with the parameter

$$s^2 = s_1^2 + s_2^2 \quad (49)$$

With regard to our considered problem, namely the scatter of electrons in a target, it is interesting to note that by a deconvolution with the parameter  $s_2$  we are able to obtain the source, which itself results from a convolution with  $s_1$ . This property follows from the description of an impinging electron current to a target by a proper Gaussian distribution (with  $s_1$  as half-width value parameter) instead of a  $\delta$ -function localized at a point with  $x = y = z = 0$ .

For the following, the operator notations of the Gaussian kernel  $K$  and its inverse kernel  $K^{-1}$  represent useful tools. These operator notations are nothing but operator functions, and their power expansions are Lie series of operators. However, these notations can only be applied to smooth functions, i.e. it is possible to perform differentiations up to arbitrary order  $n$  ( $n \Rightarrow \infty$ ). This property implies the function class  $C^\infty$ , which has to be subjected to the differential operator formulation. The Gaussian kernel  $K$  can be derived as a Greens function of the operator function (Ulmer 1980, 2010):

$$\varphi = F(\Delta) \cdot \Phi = \exp(0.25 \cdot s^2 \cdot \Delta) \cdot \Phi \quad (50)$$

or

$$\varphi(x, y, z) = \iiint K(s, u-x, v-y, w-z) \Phi(u, v, w) du dv dw \quad (51)$$

The 3D-kernel  $K$  is defined as above, and  $\Delta$  is the 3D Laplace operator. It should be noted that from the theory of integral equation is known that a two-point integral kernel is always equivalent to a certain differential operator acting in a differential equation.

It has to be added that the parameter  $s$  has not to be identical for all three dimensions. This is important with regard to the preference direction  $z$  of our task. Thus we distinguish between  $x/y$  plane and  $z$  direction. The parameter  $s$  is now restricted to the  $x/y$  plane and for the  $z$  direction we use the parameter  $\sigma$ . By that, equations (50 – 51) now read:

$$\varphi = F(\Delta) \cdot \Phi = \exp[0.25 \cdot [s^2 \cdot (\partial^2 / \partial x^2 + \partial^2 / \partial y^2) + \sigma^2 \cdot \partial^2 / \partial z^2]] \cdot \Phi \quad (52)$$

or

$$\varphi(x, y, z) = \iiint K((s, u - x, v - y), (\sigma, w - z)) \Phi(u, v, w) du dv dw \quad (53)$$

In explicite calculations we have to account for this distinction, and only for brevity we often refer to one parameter for all 3 dimensions.

Eq. (50) has a very important quantum theoretical background (Ulmer 2010, Ulmer and Matsinos 2010). It results from an exchange Hamiltonian (Schrödinger equation) and its coupling to a Boltzmann equation (canonical ensemble):

$$\left. \begin{aligned} \varphi &= \exp(-H / E_{ex}) \Phi = F_H \Phi \\ F_H &= \exp(-H / E_{ex}) \end{aligned} \right\} \quad (54)$$

The operator  $F_H$  is connected to the Schrödinger Hamiltonian by the following way:

$$\left. \begin{aligned} H &= -\frac{\hbar^2}{2m} \Delta \\ \exp(0.25 \cdot s^2 \Delta) \Phi &= F_H \Phi = \varphi \\ s^2 &= 2\hbar^2 / (mE_{ex}) \end{aligned} \right\} \quad (55)$$

$E_{ex}$  incorporates the exchange energy in the medium, which finally transforms  $\Phi$  to  $\varphi$ . The kernel  $K$  represents the Greens function of the operator  $F_H$ . This can be verified by the spectral theorem of functional analysis:

$$\left. \begin{aligned} F_H \Phi &= \gamma \Phi \\ \Phi_k &= \exp(-ikz) / \sqrt{2\pi}^3 \\ F_H \Phi_k &= \gamma(k) \exp(i\vec{k} \cdot \vec{x}) / \sqrt{2\pi} = \exp(-s^2 \vec{k}^2 / 4) \cdot \exp(i\vec{k} \cdot \vec{x}) / \sqrt{2\pi}^3 \\ K(s, u - x, v - y, w - z) &= \int \Phi_k^*(\vec{x}) \Phi_k(\vec{u}) \gamma(k) d^3k = \\ &= \frac{1}{(2\pi)^3} \int \exp(-s^2 \vec{k}^2 / 4) \exp(i\vec{k}(\vec{u} - \vec{x})) d^3k \\ K(\sigma, u - z) &= \frac{1}{s^3 \sqrt{\pi}^3} \exp(-(\vec{u} - \vec{x})^2 / s^2) \end{aligned} \right\} \quad (56)$$

The contents of Equations (52 – 53) would result from the fact that in the x/y plane we have to deal with the exchange energy  $E_{ex}$  expressed by the parameter  $s$ , whereas in z direction a different exchange energy  $E_{ex}$  has to be accounted for, which yields the parameter  $\sigma$ . The contributions in

the x/y plane of the above kernel can be interpreted as multiple scatter, if restricted to one Gaussian kernel. The different part in z direction represents either energy fluctuation, if  $\sigma$  is real, or energy fluctuation combined with energy dissipation, if  $\sigma$  has a complex value. This implies transition of electron kinetic energy to radiation energy and energy loss described phenomenologically by Eq. (43). If we use linear combinations of Gaussian kernels in order to account for tails (see e. g. Ulmer et al 2005) the related inverse problem has also been worked out (Ulmer 2010).

It should be noted that there are significant generalizations of Eqs. (54 – 56) possible, which imply that the simple Gaussian kernel has to be modified by certain Hermite polynomials or by linear combinations of different Gaussian kernels to account for tails (see above note). Thus for brevity, we only write the formulas in one space dimension.

Owing to the linearity of  $F_H$ , that is, the absence of terms of the form  $(F_H \cdot \Phi)^2$ , the solution function  $\Phi_k = \exp(-i k z) / \sqrt{2\pi}$  is not the only possible one; the multiplication with an arbitrary function  $g(k)$  also solves Eq. (56):

$$\Phi_k = g(k) \exp(-i k z) / \sqrt{2\pi} \quad (57)$$

The power expansion (57) and the application of the spectral theorem (56) lead (for each power  $k^n$ ) to the set:

$$f(k) = g * (k) g(k) = a_0 + a_1 k + a_2 k^2 + \dots + a_n k^n \quad (58)$$

We perform the substitutions:

$$\left. \begin{aligned} k' &= k - 2i(u - z) / \sigma^2 \quad (59) \\ \int k'^n \exp(-k'^2 / a) dk' &= \Gamma((n+1)/2) / (2 \cdot a^{(n+1)/2}) \quad (60) \end{aligned} \right\}$$

With the help of relation (60), we obtain the kernel expansion:

$$\begin{aligned} K(\sigma, u - z) &= \sum_{n=0}^N a_n \sum_{j=0}^n \binom{n}{j} \Gamma((j+1)/2) \left( \frac{1+(-1)^j}{2} \right) (\sigma^2 / 4)^{-(j+1)/2} (2i(u - z) / \sigma^2)^{n-j} \cdot \\ &\quad \cdot \exp(-(u - z)^2 / \sigma^2) / 2\pi \quad (61) \\ &\quad (N \rightarrow \infty) \end{aligned}$$

Every finite sum running from 0 to N ( $N < \infty$ ) is also a solution. In particular,  $N = 0$  provides the familiar Gaussian kernel. A rather similar expression can be derived by a Boltzmann equation; the resulting kernel can be rewritten in terms of a Gaussian multiplied with Hermite polynomials (in one dimension, see Ulmer (1980, 1983)):

$$\left. \begin{aligned} K &= \sum_{n=0}^N B_n(\sigma) \cdot \left(\frac{u-z}{\sigma}\right)^n \cdot \exp\left(- (u-z)^2 / \sigma^2\right) \Rightarrow \\ K &= \sum_{n=0}^N P_n(\sigma) \cdot H_n\left(\frac{u-z}{\sigma}\right) \cdot \exp\left(- (u-z)^2 / \sigma^2\right) \end{aligned} \right\} \quad (62)$$

(lim  $N \rightarrow \infty$ )

One should note that there is a rigorous correspondence between ordinary polynomials and Hermite polynomials. By that, we are able to express  $B_1$  in terms of  $P_0, P_1, \dots, P_1$  (see Abramowitz and Stegun 1970). Although the basis of Eq. (62) is of quantum-mechanical nature, it can readily be interpreted as a general solution of the Boltzmann equation, where the two-point polynomials refer to the corresponding order of statistical moments ( $N$  may be kept finite). This provides a connection to Grad's solutions, which have often been studied in radiation physics. An interesting special case of the expansion (62) is given by:

$$f(k) = c_g + c_e \cdot \exp(\pm k / k_0) \quad (63)$$

The power series of  $\exp(\pm k/k_0)$  leads to the expansion (63) with fixed coefficients  $a_k$ ; the resulting kernel  $K$  is obtained in a straightforward manner:

$$K = [c_g \cdot \exp(-(\bar{u} - \bar{x})^2 / \sigma^2) + c_e \cdot \exp(-(\bar{u} - \bar{x} \pm 1/k_0)^2 / \sigma^2)] \frac{1}{\sigma \cdot \sqrt{\pi}} \quad (64)$$

The minus sign before the term  $1/k_0$  in the previous equation implies a shift to a lower energy and reverse; the normalization condition of the kernel  $K$  is  $c_g + c_e = 1$  and other properties such as  $\sigma_n^2 = n \cdot \sigma^2$  also hold, if the convolution is repeated  $n$  times. The Gaussian convolutions and their generalizations developed in this section represent Poisson distributions in the energy space, as may be verified easily by the operator  $F_H \Phi = \exp(-H/E_{ex}) \Phi = \exp(-E/E_{ex}) \Phi$ . A further generalization results from the Dirac equation and Fermi-Dirac statistics (see also the formula  $q(\theta)$  in scatter theory inclusive

form factor in the previous section):

The Dirac equation in differential operator version of Eq. (8) is obtained by the substitution  $\vec{p} \Rightarrow \frac{\hbar}{i} \cdot \nabla$  :

$$(\beta mc^2 + \frac{\hbar c}{i} \cdot \vec{\alpha} \cdot \nabla) \psi = E_D \cdot \psi \quad (65)$$

According to Feynman (1962),  $E_D$  satisfies the relation:

$$E_D = \pm mc^2 \sqrt{1 + 2 \cdot E_{Pauli} / mc^2} \quad (66)$$

$E_{Pauli}$  is the energy of the related Pauli equation, and, if we neglect spin effects, we can replace  $E_{Pauli}$  by  $E_{Schrödinger}$ . Since the energy level, required for the creation of positrons, is distant to the available  $E_{max}$  value, we also omit the minus sign in Eq. (66). With respect to the Fermi-Dirac statistics, we use the notation  $\hat{H} = H_D - E_F$  ( $E_F$ : energy of the Fermi edge). The Fermi distribution function is:

$$f_F(\hat{H}) = f(\hat{H}) \cdot d_s(H_D) \quad (67)$$

The notation  $d_s(H_D)$  refers to the density of states corresponding to the energy  $E_D$  (or Hamiltonian  $H_D$ ) and  $E_F$  to the Fermi edge. By use of these definitions, the operator equation of Fermi-Dirac statistics, which will be used, assumes the shape:

$$f_F(\hat{H}) = \frac{1}{1 + \exp((H_D - E_F) / E_{ex})} \cdot d_s(H_D) \quad (68)$$

Since the relation (68) considerably simplifies a lot of calculations, we have to recall that, for the eigenvalues  $E$  of *continuous* operators  $H$ , the following property is valid:

$$\left. \begin{aligned} H \psi &= E \psi \\ f(H) \psi &= f(E) \psi \end{aligned} \right\} \quad (69)$$

The operator function  $f(H)$  may result from an iteration of  $H$  (Lie series) as already used with regard to the Schrödinger equation. With the restriction to the z-axis and n-times repetition of the Fermi

operator  $f_F(\hat{H})$ , we obtain:

$$\left. \begin{aligned} \eta(k) &= [mc^2 \sqrt{1 + \hbar^2 \cdot k^2 / m^2 c^2} - E_F] / E_{ex} \\ \gamma(\eta(k)) &= [\frac{1}{2}(\eta \cdot E_{ex} + E_F) / mc^2]^n \cdot \exp(-n\eta / 2) \cdot \sec h(\eta / 2)^n \end{aligned} \right\} \quad (70)$$

The general convolution kernel  $K_F$  is given by:



$$K_F = \frac{1}{2\pi} \cdot \int_{-\infty}^{\infty} \exp(i\vec{k}(\vec{u} - \vec{z})) \cdot d\gamma(\eta(\vec{k})) \quad (71)$$

This integral cannot be evaluated by elementary methods, but it is possible to expand the hyperbolic-secant function  $\text{sech}(\eta/2)$  in terms of a Gaussian multiplied with a specific power expansion. By that, we obtain a rigorously generalized version of the nonrelativistic kernels. Thus, it is known from mathematical textbooks that the polynomial expansion of  $\text{sech}(\xi)$  is given by:

$$\text{sech } h(\xi) = \sum_{l=0}^{\infty} E_{2l} \cdot \xi^{2l} / (2l)! \quad (|\xi| < \pi/2) \quad (72)$$

$E_{2n}$  are the Euler numbers; because of the very restricted convergence conditions, this expansion does not help. In view of the evaluation of the kernel  $K_F$ , we have derived a more promising expansion without any restriction for convergence:

$$\left. \begin{aligned} \text{sech } h(\xi) &= \exp(-\xi^2) \cdot \sum_{l=0}^{\infty} \alpha_{2l} \cdot \xi^{2l} \\ \alpha_{2l} &= E_{2l} / (2l)! + \sum_{l'=1}^l (-1)^{l'+1} \cdot \alpha_{2l-2l'} / l'! \end{aligned} \right\} \quad (73)$$

The coefficients  $\alpha_{2l-2l'}$  are recursively defined. Some low-order coefficients are:  $\alpha_0 = 1$ ,  $\alpha_2 = 1/2$ ,  $\alpha_4 = 5/4!$ ,  $\alpha_6 = 29/6!$ ,  $\alpha_8 = 489/8!$ . It is easy to verify that, due to the Gaussian, the expansion above converges for  $|\xi| \leq \infty$ . Since  $\eta(k)$  is given by a root, some terms are connected with difficulties, but if we expand  $\eta(k)$  by the power expansion, then – besides the rest energy  $mc^2$  – the first expansion term is the nonrelativistic contribution; thus, we may consider only Fermi statistics without relativistic terms (Dirac). The higher-order terms are now readily evaluated (up to arbitrary order). The energy distribution function  $S_E$  assumes the shape:

$$S_E = N_f \cdot \exp(-(E_n(k) - E_{\text{Average},n})^2 / 2\sigma_E(n)^2) \cdot \sum_{l=0}^{\infty} b_l(n, mc^2) \cdot (E_n(k) / 2E_{ex})^l \quad (74)$$

$N_f$  is a normalization factor. Eq. (74) provides a very interesting special case: if we take  $l = 0$  and real values of  $\sigma_E$ , we obtain Bohr's classical formula and a connection between  $E_{\text{Average}}$  and  $E_F$  (Ulmer and Matsinos 2010). The convolution kernel  $K_F$  is determined by the general structure (in one dimension):

$$K_F = N_f \cdot \sum_{l=0}^{\infty} H_l((u - z - z_{\text{shift}}(l)) / \sigma_n) \cdot B_l(n, mc^2) \cdot \exp(-(u - z - z_{\text{shift}}(l))^2 / 2\sigma_n^2) \quad (75)$$

Now  $E_{\text{Average}}$  and  $z_{\text{shift}}$  depend in any order on the Fermi edge energy. Detailed descriptions of the above terms are avoided in this paper; Formulas (74 – 75) represent only a general outline. If we recall that  $\sigma_n$  is a function of  $z$  (that is,  $\sigma(z)$ ), and take the proportionality  $E_F \sim E_{\text{Average}}$  into account, we can verify that the Landau – Vavilov theory represents a specific form of a Fermi-Dirac distribution. It should also be emphasized that  $E_F$  and consequently  $E_{\text{Average}}$  depend on the electron track, but in a low order (that is, the electron energy is  $E_0 \approx mc^2$  and the kinetic energy  $E_\delta$  of  $\delta$ -electrons satisfies  $E_\delta \ll 2mc^2$ ), the Bohr approximation formula is a good basis. For homogeneous media, this simplification works, since the residual energy  $E(z)$  of a electron is monotonically decreasing in the cone target. (For heterogeneous media, we have always to take slabs with different densities and material properties like  $\sigma_{\text{Tungsten}}$  and  $(Z/A)_{\text{Tungsten}}$  into account.) The question arises as to when the kernel  $K_F$  can be used. The first case pertains to the energy/range straggling of fast electrons as primary projectiles; to avoid unnecessary evaluations of higher order, it is necessary to check the order of  $K_F$  by comparison to the measured stopping power. The second case is the calculation of transition probabilities and of the energy transfer of electrons passing in the environment of heavy nuclei (production of bremsstrahlung). The Pauli principle for spin gives raise to exchange interactions. In agreement with a previous publication we restrict ourselves to the case of two Gaussian kernels, which have partially deconvolved under influence of a magnetic field. The extension of the operator  $F_H$  by inclusion of a magnetic field (i.e. vector potential  $\mathbf{A}$ ) will be presented here for the case according to Eqs. (46 – 53).

The inverse differential operator of the above operator function (38) is rather simply given by:

$$F^{-1}(\Delta) = \exp(-0.25 \cdot s^2 \cdot \Delta) \quad (76)$$

Both operators satisfy the condition  $F \cdot F^{-1} = F^{-1} \cdot F = 1$  (unit operator). However, the application of  $F(\Delta)$  to functions obtained by Fourier transforms represents a useful tool, and even the kernel  $K$  acting as a Greens function can be derived in that manner. On the other side, the application of  $F^{-1}$  to function systems, obtained by Fourier transforms, does, in general, not exist and may lead to awkward problems (Ulmer 2010). However, we are able to write down the following properties:

$$F^{-1}(\Delta) = \exp(-0.25 \cdot s^2 \cdot \Delta) = \exp(0.25 \cdot s^2 \cdot \Delta) \sum_{n=0}^{\infty} (-1)^n \cdot s^{2n} / (n! \cdot 2^n) \cdot \Delta^n \quad (77)$$

Since the operator  $F(\Delta)$  provides the Gaussian kernel  $K$ , the application of this expansion of  $F^{-1}$  provides the Gaussian kernel  $K$  multiplied with a sequence of Hermite polynomials as stated above. This fact follows from the differentiations of  $K$  by  $\Delta^n$ , providing Hermite polynomials of even

order. Thus a formal reduction of scatter from the state  $s^2 = s_1^2 + s_2^2$  to the state  $s_1^2$  requires a convolution with regard to  $s^2$  and a deconvolution with regard to  $s_2^2$  to yield the initial state with  $s_1^2$ :

$$F^{-1}(0.25s_2^2\Delta) \cdot F(0.25s^2\Delta) = \exp(0.25s_1^2 \cdot \Delta) \quad (78)$$

5 This provides the distribution function of the source state, e.g. initial fluence distribution function of the impinging electrons.

However, this is only a formal reduction, and we have not yet determined a calculation procedure for the description of electron in an inhomogeneous magnetic field with focusing properties, if the electrons leave the first subtarget (or any other target). This goal can also be solved with the presented formalism. In the presence of a magnetic field, described by the vector potential  $\mathbf{A}$  (or the magnetic induction  $\mathbf{B} = \text{curl } \mathbf{A}$ ), we have to perform a gauge-invariant modification ( $\mathbf{A}$  has also to satisfy  $\text{div} \mathbf{A} = 0$ ). The magnetic induction  $\mathbf{B}$  contains the magnetic field strength  $\mathbf{B}$  resulting from the current in a solenoid and the ferromagnetic material. The gauge-invariant operator  $F$  reads:

$$15 \quad F(\vec{A}, \Delta) = \exp[0.25 \cdot s^2 \cdot (\nabla - e/(D \cdot \mathbf{m} \cdot \mathbf{c}) \cdot \vec{A})^2] = \exp[0.25 \cdot s^2 \cdot (\Delta + \beta^2 \vec{A}^2 - 2 \cdot \beta \cdot \vec{A} \cdot \nabla)] \quad (79)$$

$$\beta = e/(m \cdot c \cdot D)$$

This formula contains a sum of different operator functions in the exponential function. With the help of the Weyl-relation we are able to transform the above expression in products, i.e. if  $\mathbf{A}'$  and  $\mathbf{B}'$  are non-commuting operators, then  $\exp(\mathbf{A}' + \mathbf{B}') = \exp(\mathbf{A}') \cdot \exp(\mathbf{B}') \cdot \exp[-0.5 \cdot (\mathbf{A}'\mathbf{B}' - \mathbf{B}'\mathbf{A}')]$ . If we then can find a certain  $z = z_1$  for the first target plate, where the above operator function agrees with that of the inverse operator  $F^{-1}$  (without magnetic field), we have solved the task, and all other operations (bremsstrahlung production, scatter, etc.) can be repeated in the next subtarget. By the knowledge of  $\mathbf{A}$  (vector potential) or  $\mathbf{B}$  (induction) we can repeat the calculation of all processes (in particular the phase space for Monte-Carlo calculations with GEANT4). Formula (79) must be equated to an inverse operator formula, which can be satisfied for a certain  $z = z_1$ :

$$25 \quad \exp[0.25 \cdot s^2 \cdot (\Delta + \beta^2 \vec{A}^2 - 2 \cdot \beta \cdot \vec{A} \cdot \nabla)] \approx \exp[-0.25 \cdot s_2^2 \cdot \Delta] \quad (80)$$

$$z = z_1$$

The special case  $s_1 \approx 0$ , i.e. the final state is a  $\delta$ -function, leads to the magnetic focus, which is not our problem here. From Eq. (80) follows that we can construct Greens functions for the expression on the left- and right-hand side. The right-hand side provides a Gaussian kernel and Hermite polynomials; the left-hand-side is much more complicated, but a similar expansion is not difficult to be carried out, since Gaussians with Hermite polynomials represent a complete system

of functions. Thus the conditions according to Eq. (80) appear to be rather intricate, and for constant values of  $s^2$ ,  $s_1^2$ ,  $s_2^2$  it is impossible to satisfy the right-hand side of Eq. (80), which refers to a deconvolution procedure in differential operator notation, since the vector potential  $\mathbf{A}$  is a function of  $x, y, z$ .

5 According to previous findings (Ulmer 2010) we are able to proceed in the follow way:

All equations presented here starting from Eq. (56) up to Eq. (80) can also be satisfied by that case, where the terms  $\sigma$  or  $s$  (e.g.  $s$ ,  $s_1$ ,  $s_2$ ) depend on  $x, y, z$ . With regard to the differential operator notations, e.g. Eq. (80), this can be seen immediately, as the operator  $\Delta$  is not affected. In the integral operator notation (Greens function) this behavior is reflected by the fact all integrations  
10 are carried out on  $u, v, w$  and not on  $x, y, z$ .

A Fourier expansion of  $\mathbf{A}$  with  $\text{div} \cdot \mathbf{A} = 0$  has to satisfy the boundary condition of the problem, namely the properties of the multitarget cone (see e.g. Figure 5 and Eq. (5)):

$$A_j = \left\{ \sum_{l_1=0}^N \sum_{l_2=0}^N \sum_{l_3=0}^N a_{j,l_1,2,3} \exp(i \cdot \vec{l} \cdot \vec{k} \cdot \vec{x}) \right\}_{j=1,2,3} \quad (81)$$

With regard to  $s$  and  $s_2$  have to perform the corresponding expansions:

$$\left. \begin{aligned} s &= \sum_{l_1=0}^N \sum_{l_2=0}^N \sum_{l_3=0}^N s_{l_1,2,3} \exp(i \cdot \vec{l} \cdot \vec{k} \cdot \vec{x}) \\ s_2 &= \sum_{l_1=0}^N \sum_{l_2=0}^N \sum_{l_3=0}^N s_{2,l_1,2,3} \exp(i \cdot \vec{l} \cdot \vec{k} \cdot \vec{x}) \end{aligned} \right\} 15 \quad (82)$$

On the other side, we are able to expand  $s(x, y, z)$ ,  $s_1(x, y, z)$  and  $s_2(x, y, z)$  in the same fashion like Eq. (81). Only then Eq. (80) provides a procedure to calculate the influence of a magnetic field on  
20 the scatter behavior of the electrons in the multitarget cone with continuous density  $\rho_i$ . Complex arguments of the scatter functions  $s$ ,  $s_1$  and  $s_2$  imply a yield of bremsstrahlung of the multi-layered target. The evaluation of Eq. (80) together with Eq. (81) is rather a noteworthy problem of numerical procedures. We should add that for the sake of simplicity we have restricted ourselves to the operator function of one Gaussian kernel  $K$  and its inverse kernel  $K^{-1}$ . It is evident that this  
25 might be too a strong restriction in view of the relativistic energies (see e.g. the Dirac equation in connection with Fermi-Dirac statistics, which seem to require, at least, two kernels). Only for brevity we have this restriction accounted for.

#### 2.3.4. Monte-Carlo calculations with GEANT4

GEANT4 (GEANT4- documents 2005) represents an open system of a Monte-Carlo code. Significant features with regard to our problem are creation of bremsstrahlung, multiple scatter according to Molière, heat production (Bethe-Bloch equation), energy straggling (Gaussian-Landau-Vavilov), Compton scatter of  $\gamma$ -radiation, and the actual energy/momentum of the electron after interactions leading to energy loss and change of the momentum. More sophisticated applications with regard to the refocusing of a multi-layered Tungsten target and back scatter of the cone walls (Tungsten, Tantalum, Lead) under boundary conditions require the explicit use of the differential cross-section formula  $q(\theta)$  with the form factor function  $F(\theta)$ . A further feature is the implementation of the magnetic field  $\mathbf{B}$  (i.e. vector potential  $\mathbf{A}$ ) to account for the Lorentz force along the track of the electrons according to the relation (3).

*In order to obtain a reliable statistical foundation, each Monte-Carlo run has been performed with  $500 \cdot 10^6$  histories.*

Since the figures 7 – 10 have methodical character, we should like to show them already in this section. In particular, Figure 7 has a fundamental meaning in this study, namely angle-dependence of the reflexion (back scatter) of fast electrons at wall consisting of high Z material (Tungsten, Tantalum, Lead). Although Pb shows the high Z value, the density is much smaller than that of W or Ta, and therefore according to Figure 7 we prefer Tungsten as the wall material for refocusing. In particular, Figure 7 represents the essential properties used in Figure 3.

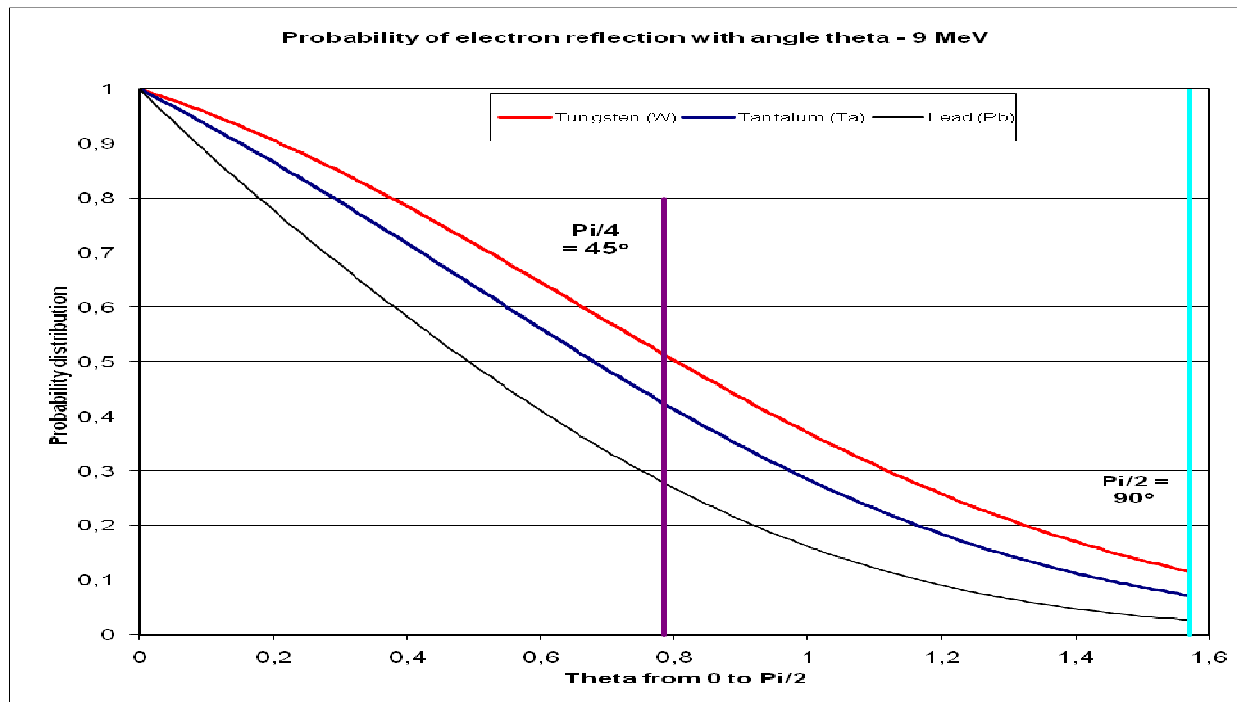


**Figure 7:** Back scatter properties (wall reflexion) of 9 MeV electrons at a high Z wall (W, Ta, Pb). The corresponding properties of 6, 18 or 20 MeV are rather similar.

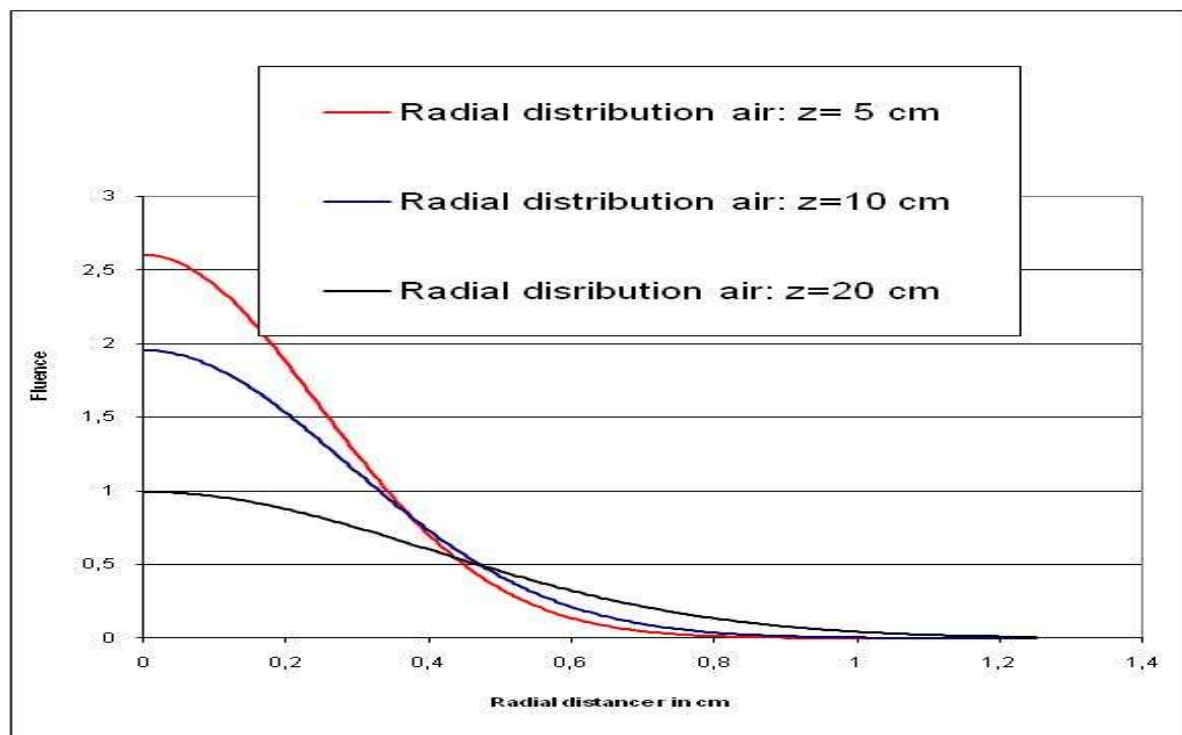


**Figure 8:** Scatter of 6 MeV electrons in air (standard conditions).

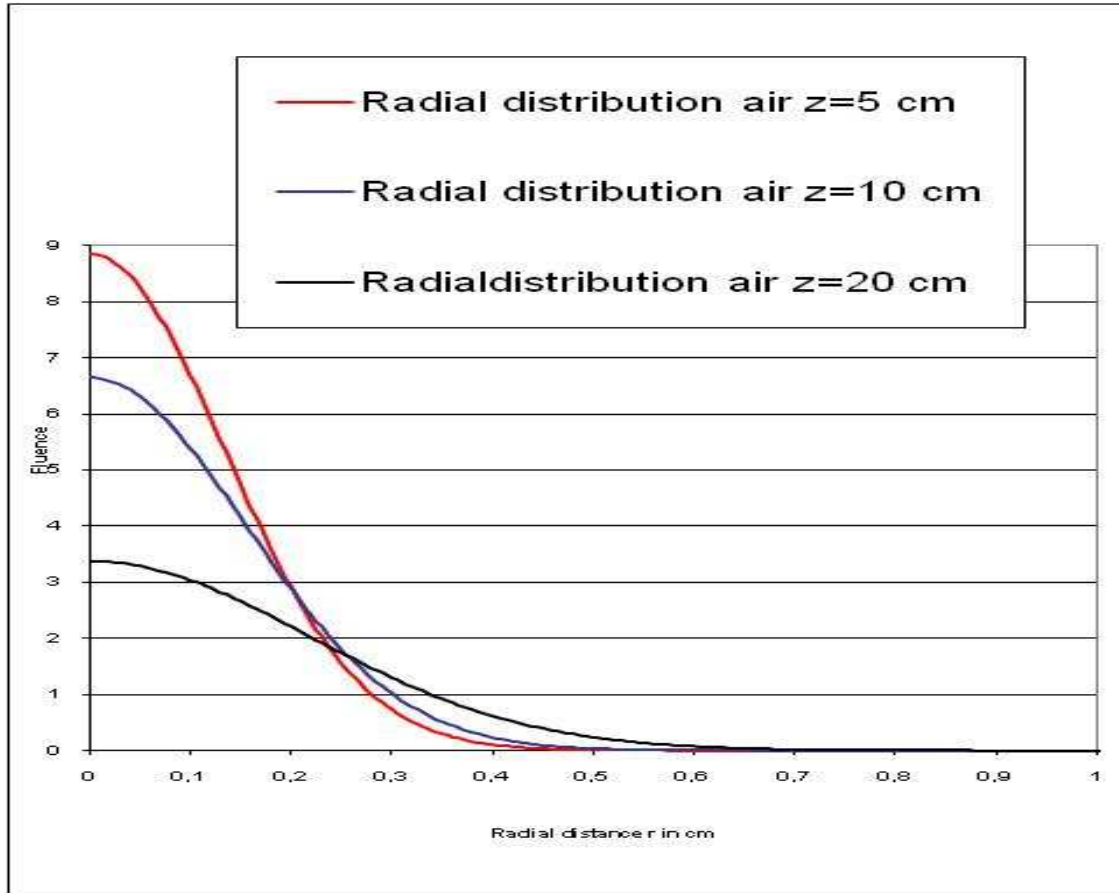


**Figure 9:** Scatter of 20 MeV electrons in air (standard conditions).

Figures 8 – 10 show the scatter behavior of fast electrons in air. In contrast to  $\gamma$ -radiation the scatter of electrons in air is not negligible. The initial condition in all 3 figures is an infinitesimally thin pencil ray of electrons. A consequence of these figures is that the multitarget has to be located in a vacuum in order to keep the lateral scatter of electrons as small as possible.

We should also point out that formula (7) would lead to a wrong behavior of reflexion of electrons (e.g. for angles smaller than  $20^\circ$ ), if the form factor function  $F(\theta)$  would have been omitted, since  $q(\theta)$  would then be highly diverging. On the other side, it is our particular interest to exploit small angle back scatter at the Tungsten wall.

At this place it should also be mentioned that a smaller refocusing effect in the multilayer cone is obtained by the Compton scatter of the  $\gamma$ -radiation, if the  $\gamma$ -quanta are scattered inside the cone. However, the refocusing of fast electrons is much more significant.

Since the refocusing via wall scatter works best with Tungsten, we do, in general, not present

calculations with other material such as Tantalum or Lead. The only exception with a Ta/Pb combination of the cone wall is restricted to one case in order to verify the preference of a Tungsten wall. In all figures of the section results we have adjusted the impinging electron beam to real conditions: The radial distribution at target surface is assumed to be a Gaussian with  $\sigma = 1$  mm:  $I(r) = I_0 \cdot \exp(-r^2/(2 \cdot \sigma^2))$ .

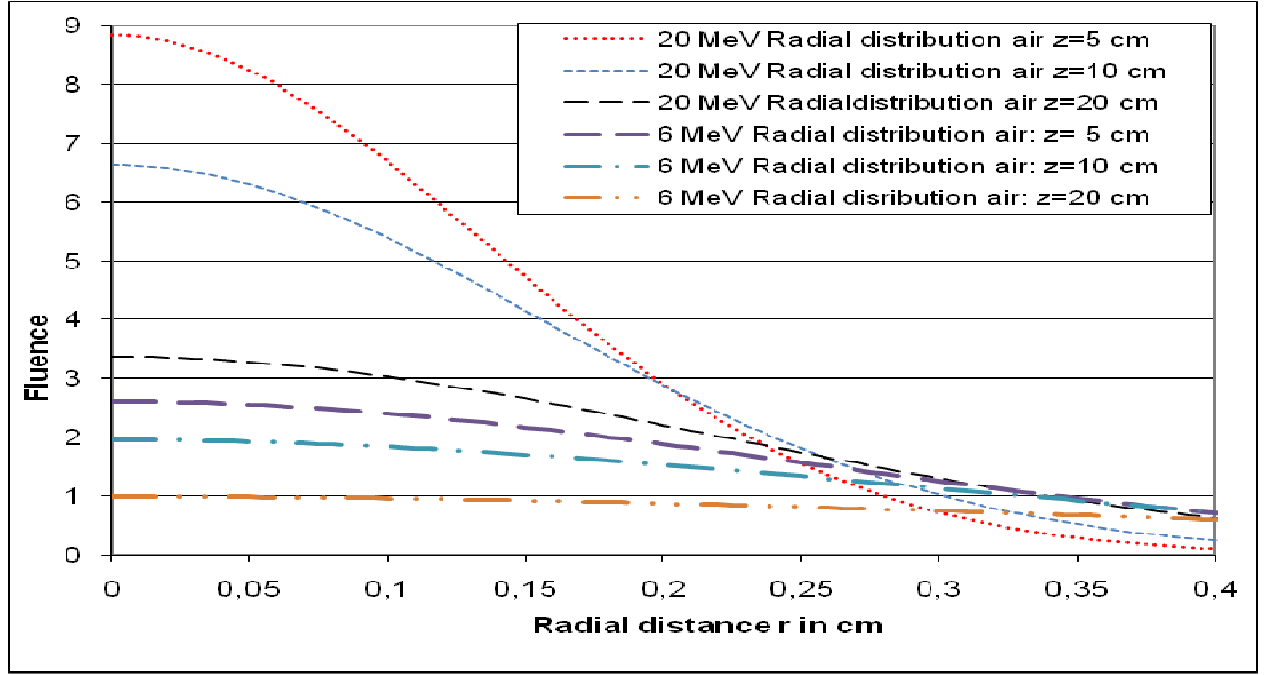


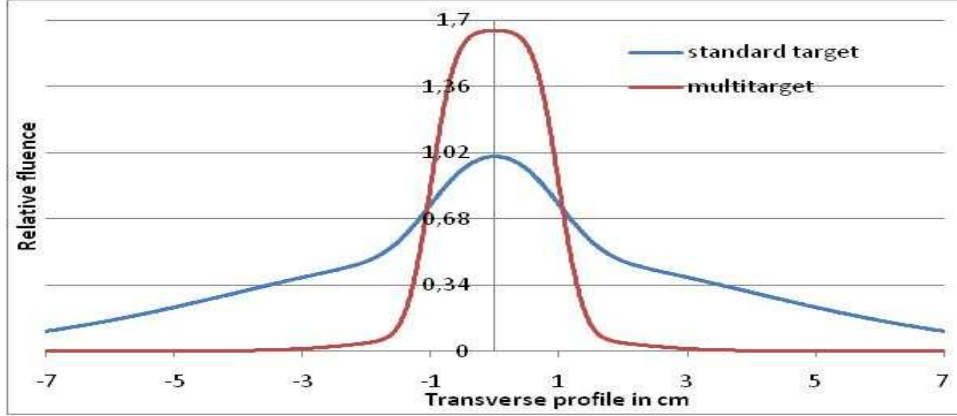
Figure 10: Comparison of air scatter of 6 MeV and 20 MeV electrons.

### 3. Results

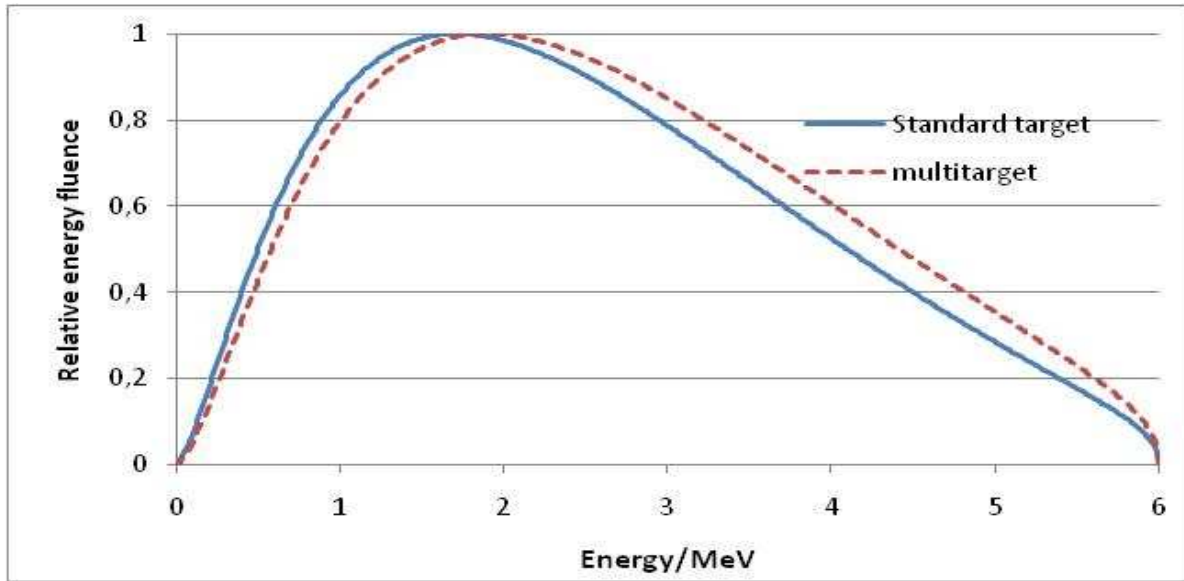
The succeeding figure 11 serves as a reference standard for all other figures. The bremsstrahlung production according to Figure 1 (blue curve, standard target) is scored along the plane immediately below the Tungsten target. The height at the central axis ( $x = y = 0$ ) is normalized to '1', and the whole behavior of the intensity distribution shows all disadvantages of the conventional target, since it decreases slowly, and even at a radius of 7 cm a noteworthy intensity has been scored. Thus the domain with  $r > 1$  cm results from multiple electron scatter in the target with no benefit for any application and requires a lot of shielding material. The behavior in the domain  $r < 1$  cm gives raise to study a multitarget cone with a radius of 1 cm at the end of the cone. The cone consists of 20 layers (distance 5 mm per layer), total depth: 10 cm, the thickness of the wall amounts to 0.02 mm Tantalum (inside) and 10 mm Lead (outside) in contrast to all other cases, where 2 mm Tungsten have been used.



The difference to the Tungsten wall (thickness: 2 mm) can be verified in Figure 14, where the case 5 corresponds to the identical condition. The case 4 is related to 100 layers with 0.01 mm thickness and 1 mm distance between each layer. The cases 1 – 3 refer to additional magnetic fields with different field strength.

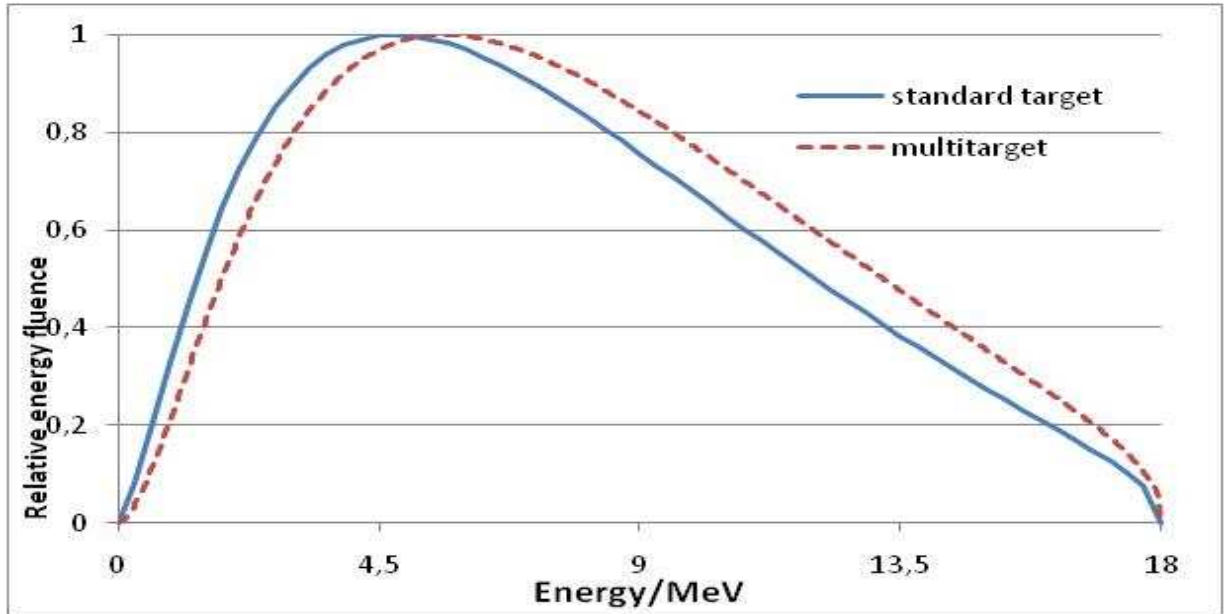


**Figure 11:** Comparison between standard target (Figure 1) and multi-layer target, electron energy  $E = 6$  MeV.

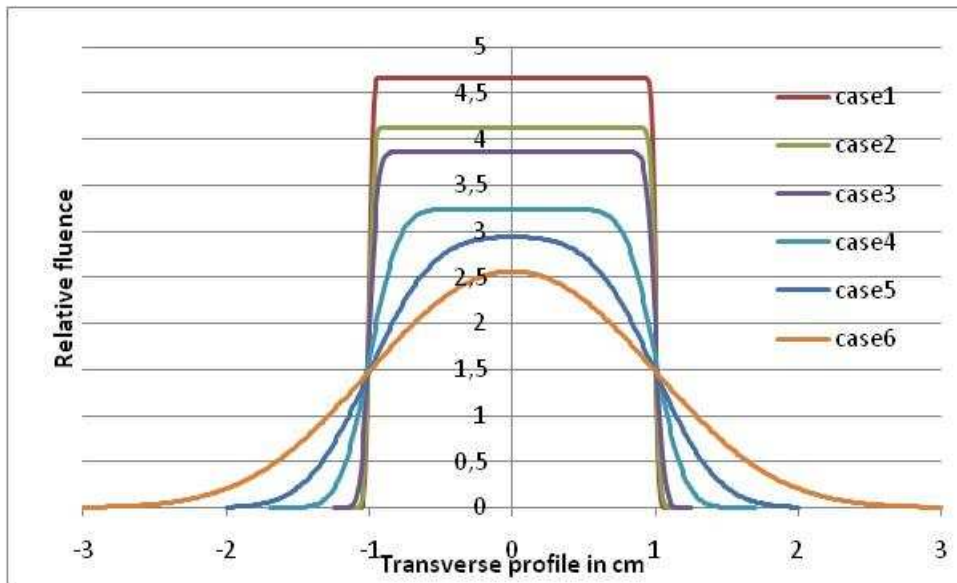


**Figure 12:** Relative energy fluence spectrum of the bremsstrahlung of 6 MeV electrons. The standard target refers to the condition presented by Ulmer et al (2005), i.e. below the flattening filter. In contrast to this condition the multitarget spectrum is scored at the end of the cone. The flattening filter is superfluous.

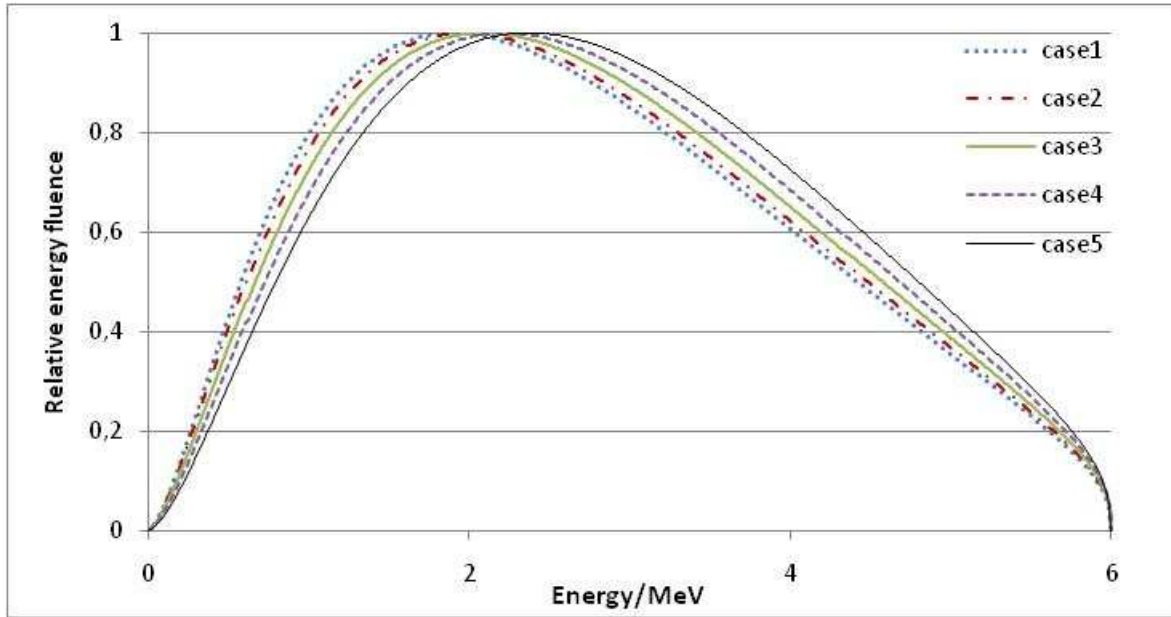
It should be pointed out that the application of  $E = 18$  MeV electron energy instead of  $E = 6$  MeV leads to rather similar properties as shown in Figure 11. Therefore we do not report them. With regard to all forthcoming Figures we use standard conditions of the cone wall, which consists of 2 mm Tungsten (with and without external magnetic field).



**Figure 13:** Relative energy fluence spectrum of the bremsstrahlung of 6 MeV electrons. The standard target refers to the condition presented by Ulmer et al (2005), i.e. below the flattening filter. In contrast to this condition the multitarget spectrum is scored at the end of the cone. The flattening filter is superfluous.

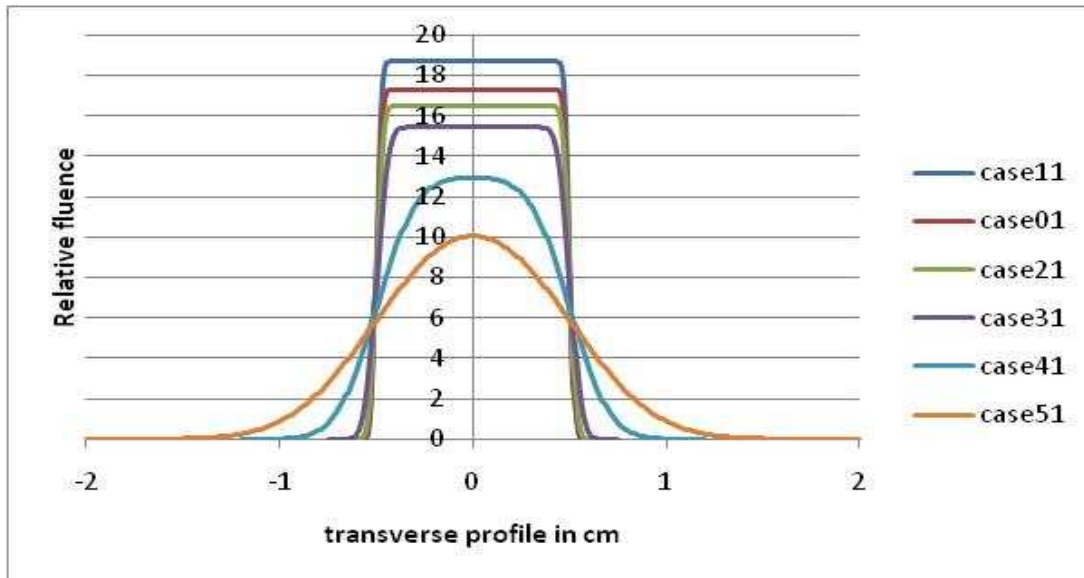


**Figure 14:** Diameter 2 cm,  $E = 6$  MeV: case 6:  $50 \times 0.02$  mm. Cases 4 - 6: without external magnetic field. Case 6:  $10 \times 0.1$  mm, case 5:  $20 \times 0.05$  mm, case 4:  $100 \times 0.01$  mm, case 3:  $100 \times 0.01$  mm, magnetic field  $m_1$  (Figure 6), case 2:  $100 \times 0.01$  mm, magnetic field  $m_2$  (Figure 6), case 1:  $100 \times 0.01$  mm, magnetic field  $m_1$  (Figure 6).



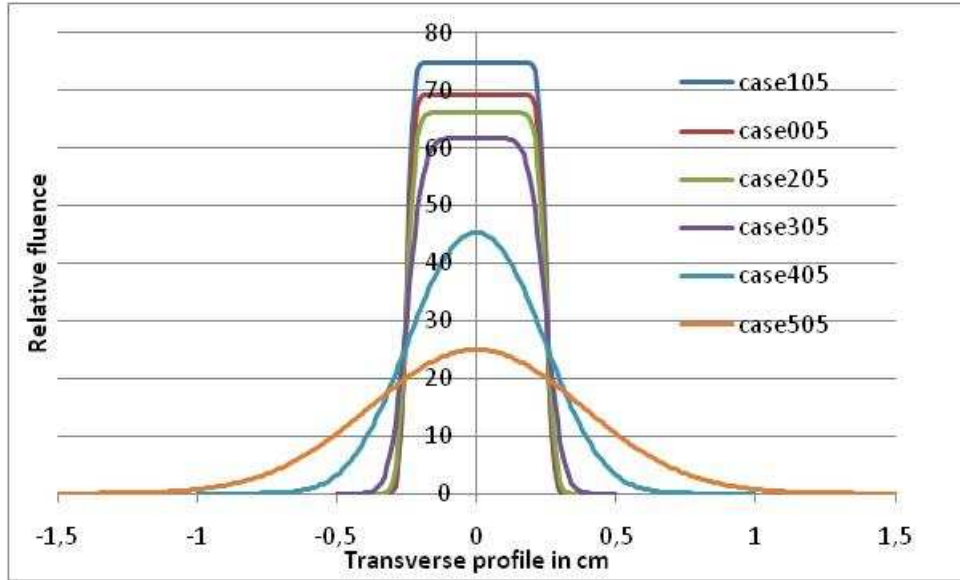
**Figure 15:** Energy spectrum of the bremsstrahlung (central ray,  $E = 6$  MeV) according to the transverse profiles of Figure 14. Case 6 of Figure 14 has been omitted.

Figure 15 clearly shows that the better the focusing of the electrons in the multitarget cone the higher is the energy spectrum. The same fact is also true with regard to the spectral properties of 18 MeV.



**Figure 16:** Diameter: 1 cm,  $E = 6$  MeV. The cases 41 (10 x 0.1 mm) and 51 (20 x 0.05 mm) have no external magnetic fields. The cases 11 – 31 refer to Figure 6: Case 31 with additional magnetic field (field strength according to  $m_1$  of Figure 6); case 21 with additional magnetic field (field strength according to  $m_2$  of Figure 6); case 01 with additional magnetic field (field strength according to  $m_3$  of Figure 6). The case 11 with the highest yield of bremsstrahlung corresponds to the case 01, but the thickness of each Tungsten layer amounts to 0.012

mm.



5 **Figure 17:** Diameter: 0.5 cm,  $E = 18$  MeV. Cases 105 – 305:  $0.01 \times 100$  mm, case 105: magnetic field  $m_3$ , case 005: magnetic field  $m_2$ , case 205: magnetic field  $m_1$ . Case 305 - 505: no magnetic field, case 405:  $20 \times 0.05$  mm, case 505:  $10 \times 0.1$  mm.

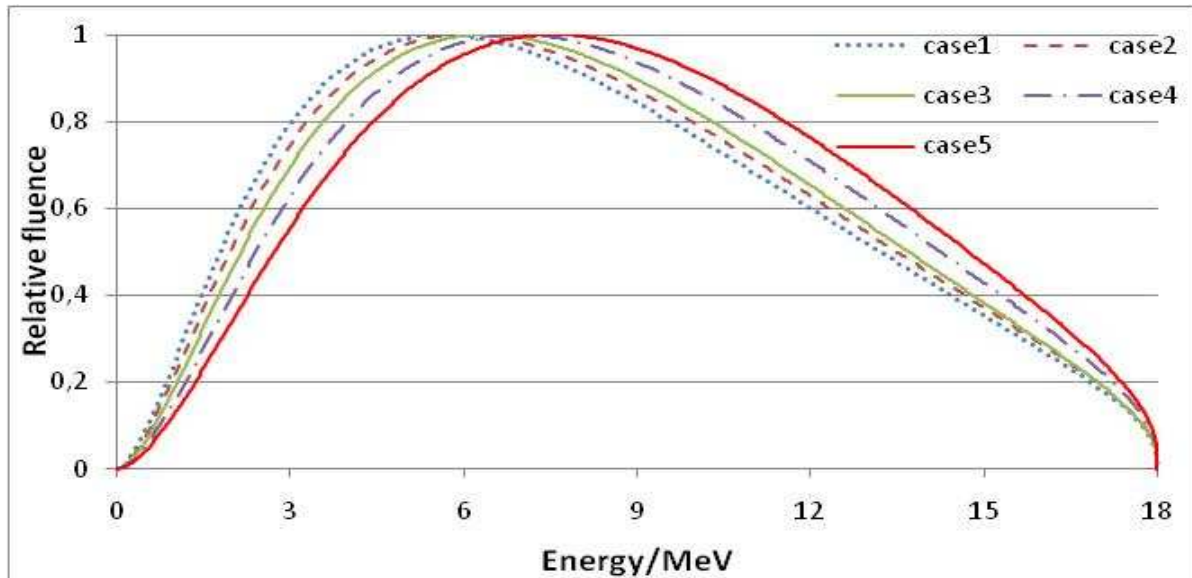


**Figure 18:** Spectral energy distribution (central ray) according to Figure 17.

10 With regard to the nomenclature it should be mentioned that cases 1, 2, 3, 4, 5 in Figure 18 correspond to cases 105, 205, 305, 405, 505 in Figure 17.

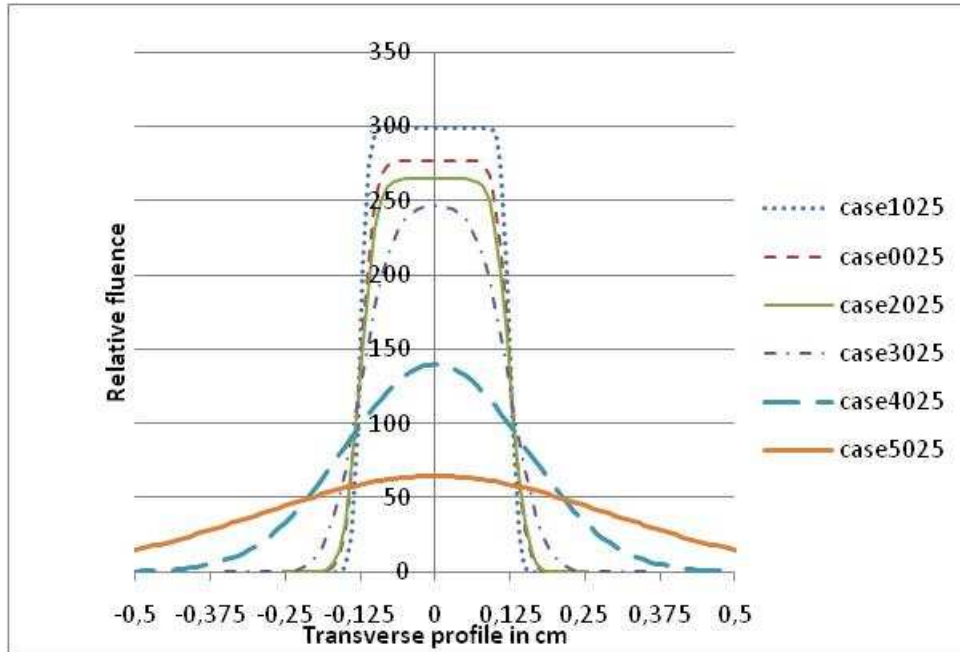


**Figure 19:** Diameter: 0.25 mm,  $E = 18$  MeV.

The nomenclature and properties of Figure 19 correspond to that of Figure 17: Cases 1025, 0025, 2025, 3025, 4025, 5025 correspond to cases 105, 005, 205, 305, 405, 505 of Figure 17.

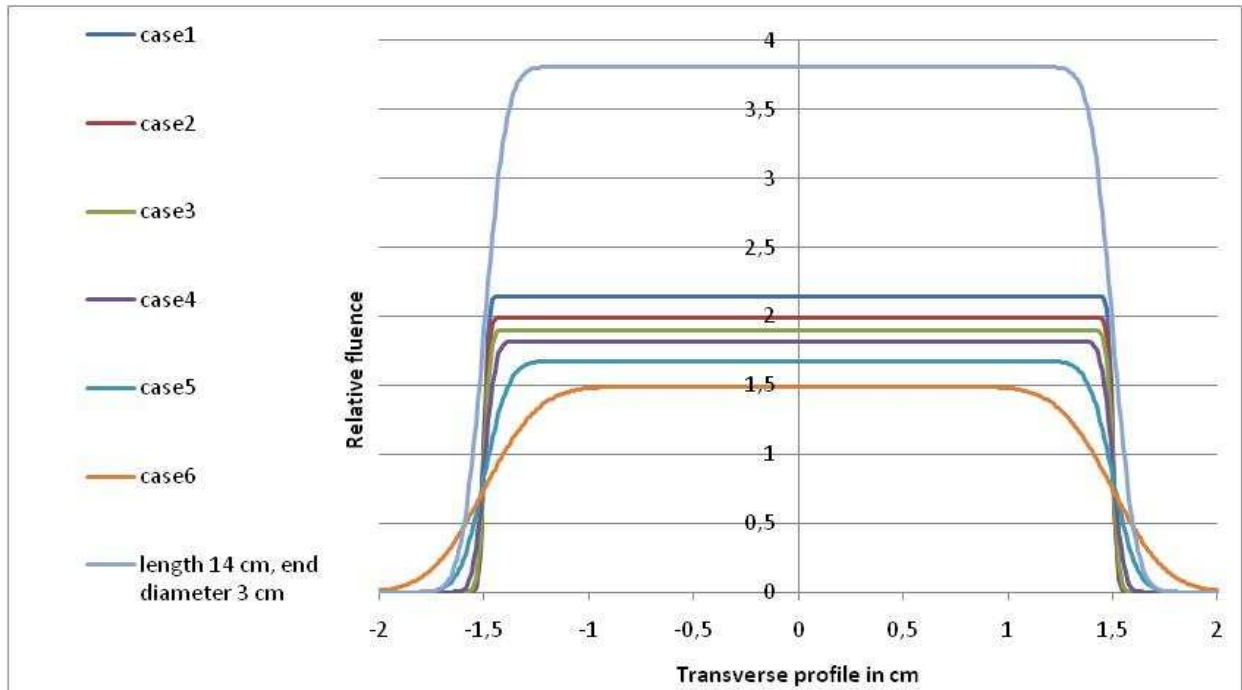


**Figure 20:** Diameter: 3 cm,  $E = 6$  MeV, depth of the cone: 14 cm. Further properties: see Figure 14.

Please note that the magnetic fields have been adapted in Figure 20 according to the geometric

properties.

With regard to research projects the deflection of the electron beam before reaching the target is often superfluous. Instead of a narrow electron beam with Gaussian half-breadth it may be more reasonable to exploit the complete energyspectrum delivered by the accelerator tube. The spectral distributions are shown in Figures 21 and 22.

5

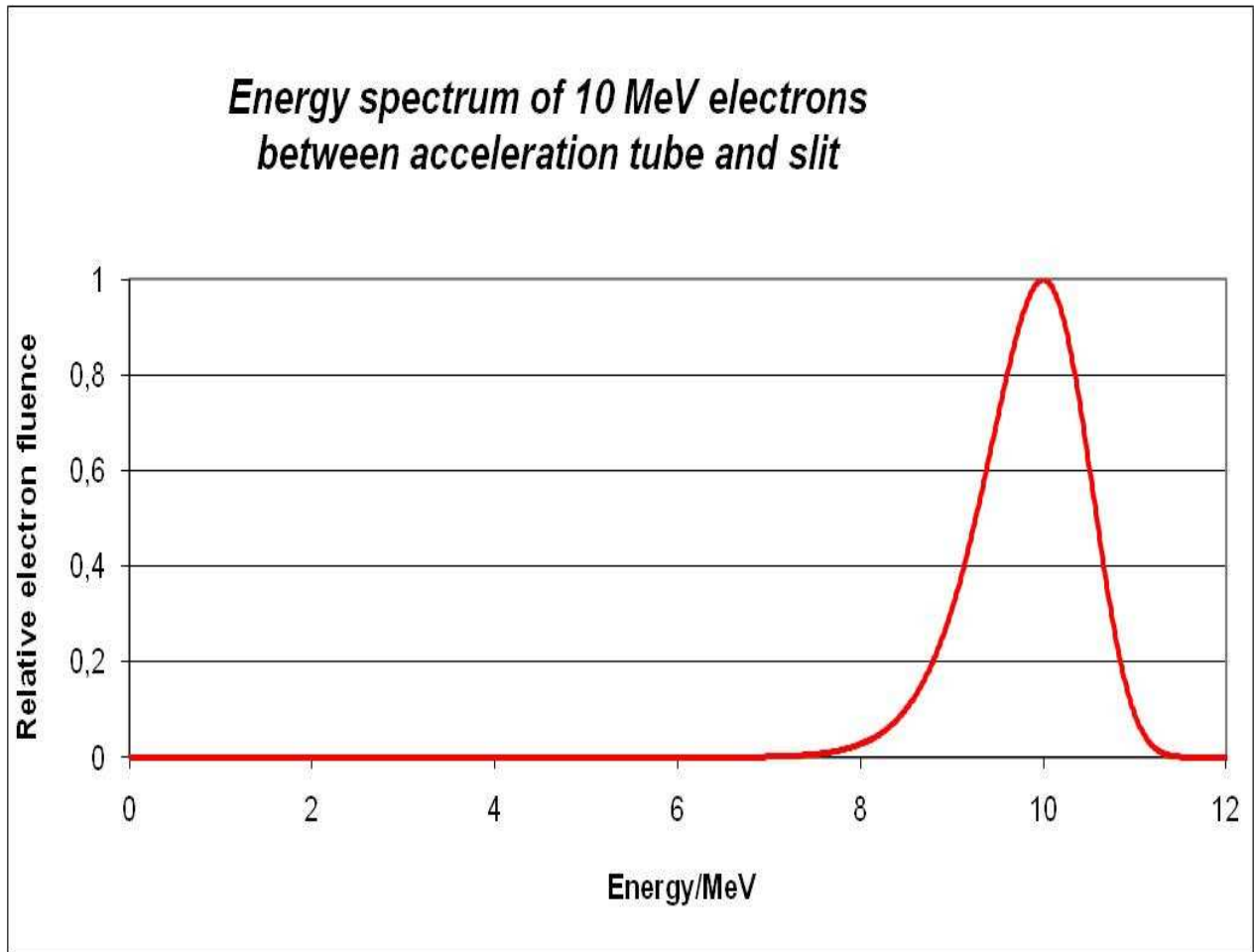


**Figure 21:** Energy spectrum after the accelerator tube for 10 MeV electrons.

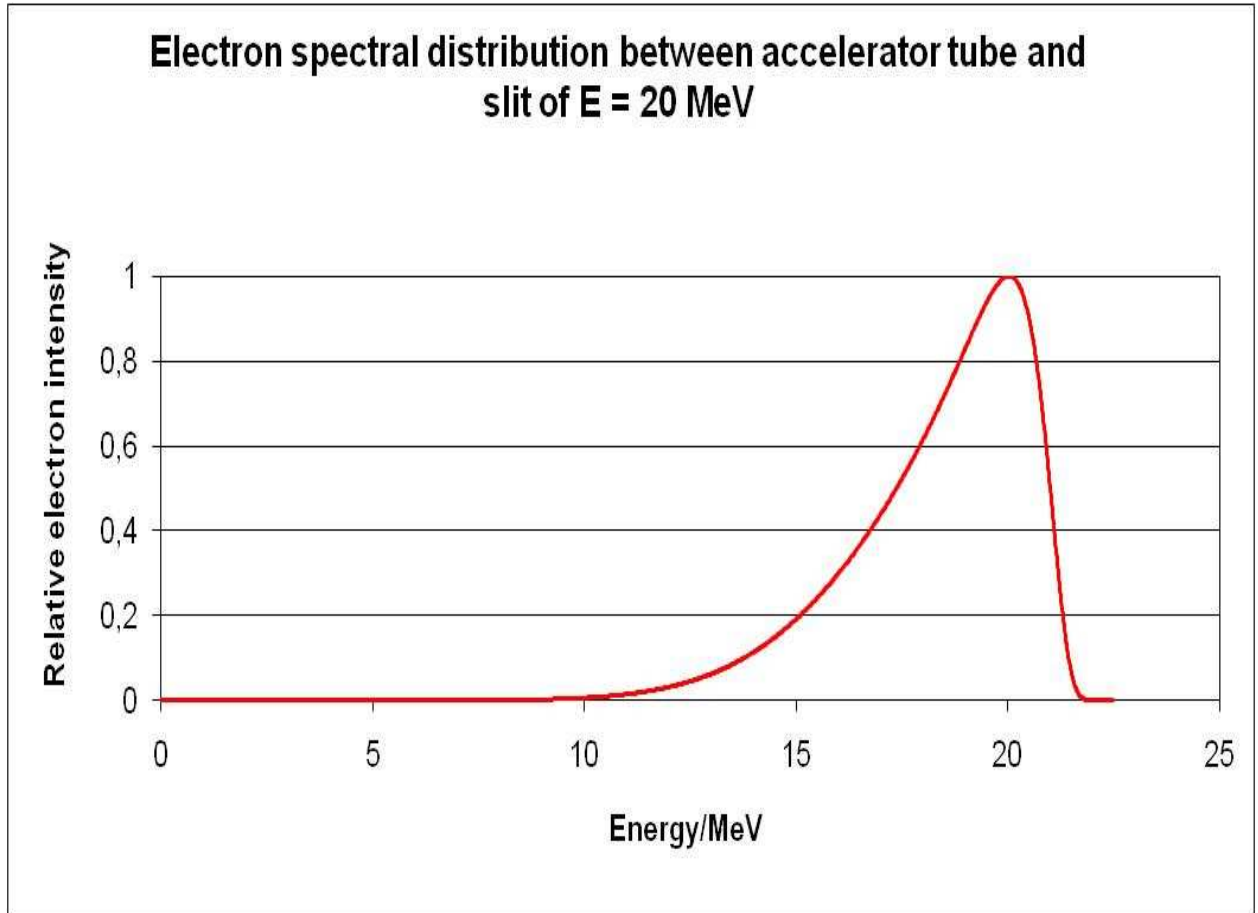


**Figure 22:** Energy spectrum of the electrons for 20 MeV.

The energy spectrum results from calculations presented by Ulmer et al (2005).

Since usual accelerators very often use the bremsstrahlung of 18 MeV, we now consider this case with regard to a very thin cone without any significant divergence (diameter at entrance: 0.24 cm, diameter at the end: 0.25 cm, depth: 20 cm, 100 x 0.01 mm Tungsten, distance between the layers: 2 mm). With regard to the external magnetic field for refocusing we have assumed the cases  $m_4$  and  $m_5$  of Figure 6.

We report here the case with the magnetic field strength  $m_4$ . It is evident that the application of the field strength  $m_5$ , which is associated with a stronger field, provides better results. The essential result is shown in Figure 23. Figure 23 stands in a close relationship to Figure 19. The energy spectrum with according normalization to '1' refers to the magnetic field strength  $m_3$ .



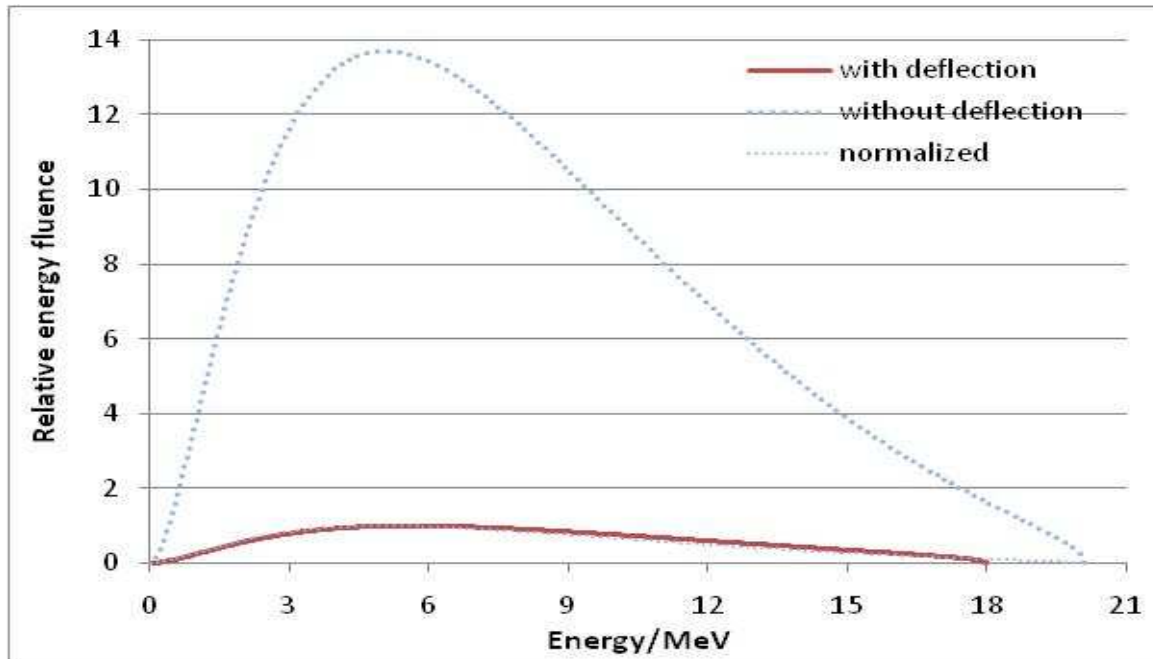


**Figure 23:** Energy spectrum of the bremsstrahlung of 18 MeV electrons. The normalization refers to the ‘narrow case’ resulting from deflection.

It should be noted that due to the lower energy components of the tube spectrum the maximum is also somewhat lower in spite of the higher magnetic field strength. On the other side, the yield of bremsstrahlung is about 14 times higher than in the case of Figure 19.

The succeeding figures 24 and 25 refer to industrial/research accelerators. In both cases it is useful to use the complete tube spectrum of an accelerator available without deflection, which we have show for 10 and MeV in Figures 21 and 22. The outcome of bremsstrahlung is desired to be very narrow (breadth ca. 4 – 5 mm without any significant divergence), but the length of the beam should be ca. 20 cm at leaving the cone. Therefore the cone has to be quite different with regard to the geometric properties and resembles a rectangular pyramid. The wall scatter of an impinging small electron beam cannot account for the desired properties of bremsstrahlung production. We assume ca. 200 plates, thickness 0.01 mm with increasing length inside the pyramidal multitarget. Thus a suitable triple quadrupole magnet can achieve the desired properties, since the small impinging beam has to be modified to a diverging elliptical beam (see Figure 24).

An alternative way is given by Figure 25. The principal difference to Figure 24 is that no triple quadruple magnet is used for distortion of the impinging electron current. A quadrupole magnet having the same construction of the pyramidal multitarget is focusing the electron beam in the narrow part and defocusing in the long part of the rectangular pyramid. The second case according to Figure 25 is much more efficient than the case of Figure 24. The yield of bremsstrahlung is about a factor 2



higher.

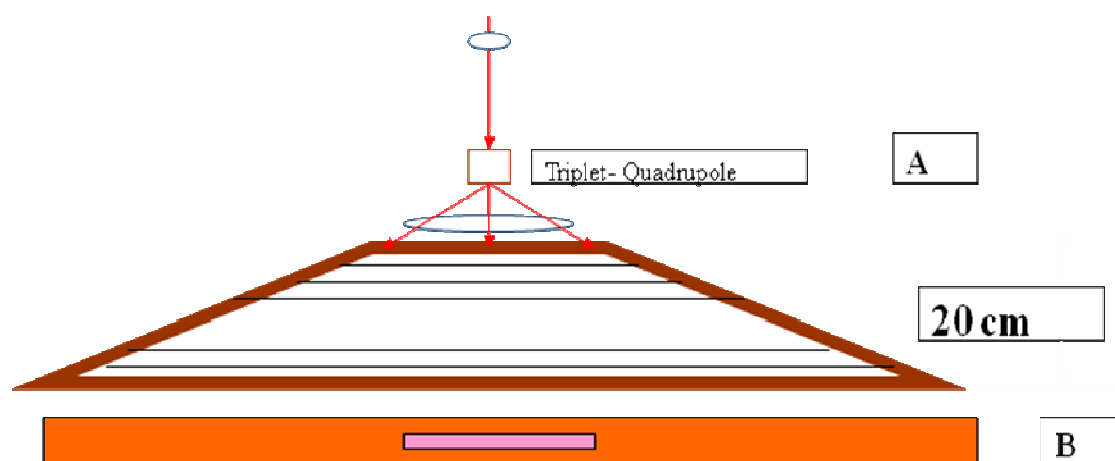


**Figure 24:** Pyramidal multitarget for the creation of a very narrow, but rather long and diverging bremsstrahlung beam.

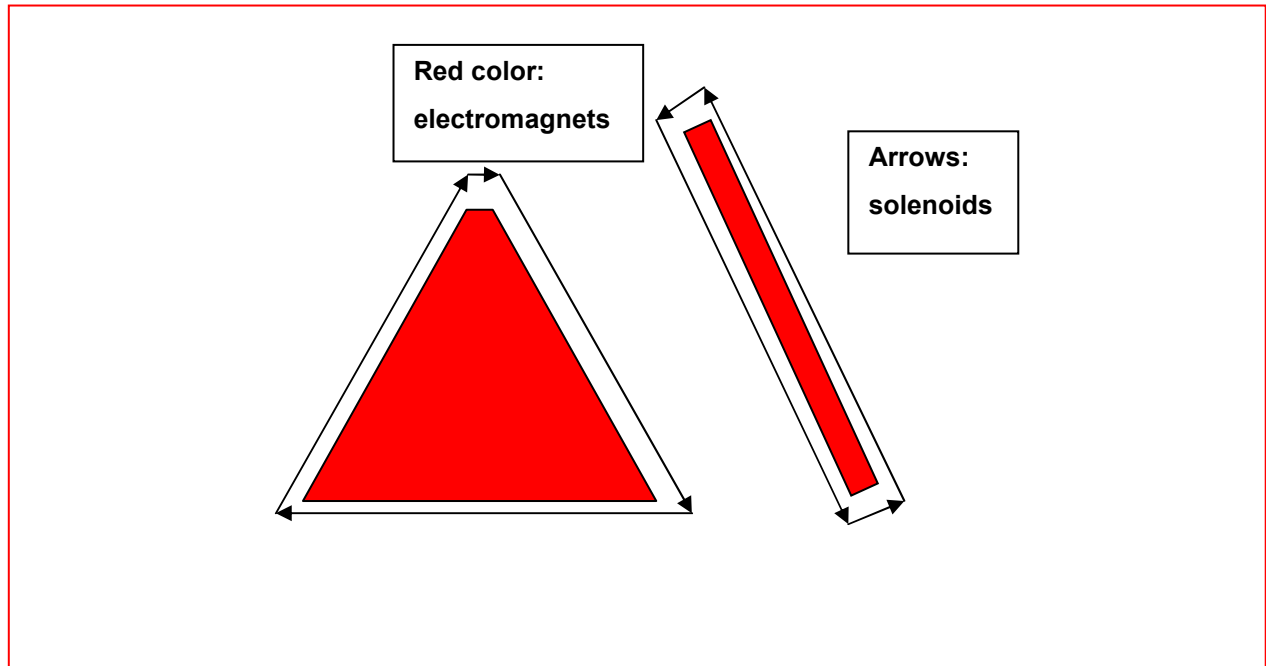


**Figure 25:** Pyramidal multitarget for the creation of a very narrow, but rather long and diverging bremsstrahlung beam. The geometrical properties are identical as in Figure 24. Only the magnet is quite different.

#### 4. Discussion

- 5 It could be shown that in conventional linear accelerators used in medicine a multitarget consisting of a Tungsten wall (thickness of the wall at least 2 mm) and ca. 100 very thin plates (thickness of a plate: ca. 0.01 mm) is superior to the standard accelerator. The bremsstrahlung beam (inclusive divergence) can be formed according to the desired properties. The energy spectrum is significantly increasing even in the absence of a refocusing magnetic field and is even better than a conventional beam, which
- 10 has passed a flattening filter. Thus the omission of such a filter provides a further yield of the factor 3 – 4. The optional amplification of the refocusing effect by suitable external magnetic fields (with regard to the required properties, see e.g. Figure 6) can be taken into account, in particular, if the outgoing  $\gamma$ -beam should be very efficient by restriction to rather small fields. These properties are important for scanning methods, stereotaxy, IMRT or tomographic applications.
- 15 The presented results also provide new doors in research, where very narrow  $\gamma$ -beams with corresponding high intensity are desired. This request cannot be satisfied without any additional magnetic field for refocusing the scattered electrons in the multitarget cone. Figures 17 and 19 show that the amplification can amount to the factor 75 (field diameter: 0.5 cm) and to the factor 300 (field diameter: 0.25 cm). By using very strong magnetic fields (case  $m_4$  or  $m_5$  of Figure 6) and the complete electron beam spectrum of the accelerator tube without deflection via bending magnet a further
- 20

amplification by a factor of ca. 13 can be achieved. The latter case is interesting for a direct measurement of the Heisenberg-Euler Compton scatter between high energy photons (see final chapter).

With regard to industrial/research applications, where a very narrow, but very long beam with high divergence is required, the configurations according to Figures 24 and 25 lead to significant improvement of the bremsstrahlung yield.

## 5. Conclusion and outlook to Heisenberg-Euler scatter

It is possible to reach some essential progress in the domain of linear accelerators in radiotherapy, since the modern irradiation techniques such as IMRT, stereotaxy, etc. do not require large field sizes, e.g. a  $40 \times 40 \text{ cm}^2$  at a distance of 100 cm from focus. This progress can be achieved by exploiting small angle reflexion of fast electrons at a Tungsten wall. The wall has to map the desired divergent properties of the beam. *A further aspect of this study is that we are able to save heavy high Z-material for the shielding of the accelerator head.*

In order to keep the scatter angles at the wall as small as possible, a multitarget with very thin Tungsten layers has to be accounted for. It is evident from electron microscopy that magnetic fields are able to amplify the refocusing properties of the wall. This refocusing amplification is absolute required with regard to the construction of a very narrow beam with correspondingly high amplification of the photon fluence and negligible divergence. For this purpose, we refer to Figures 17, 19 and 23; according to these figures a significant yield is reached. One should recall that the normalization factor '1' refers to the outcome of the conventional accelerator.

In order to check the 'so-called' Heisenberg-Euler Compton scatter via interaction of  $\gamma$ -quanta one requires two very narrow  $\gamma$ -beams according to Figure 26. According to a fundamental study on the properties of quantum electrodynamics (Euler and Kockel 1935, Euler 1936, Heisenberg and Euler 1936) the perturbation theory of 4<sup>th</sup> order provides that high energy  $\gamma$ -quanta can be mutually scattered by a 'Compton effect'. This Compton interaction results from the fundamental property that  $\gamma$ -quanta with energy significantly above the rest energy of an electron-positron pair (1.02 MeV) can undergo creation of virtual pairs and further  $\gamma$ -quanta can be scattered at these virtual pairs of electrons/positrons. In the above cited references the Lagrangian formulation of the quantized electromagnetic field is developed. The described effect also results from propagator perturbation theory of quantum electrodynamics developed by Feynman (see Feynman 1962). Since the described effect results from the scatter of light at virtual pairs, it is in contrast to electrodynamics of Maxwell, where light beams with arbitrary high energy in frequency and amplitude may cross each other

without having a mutual influence.

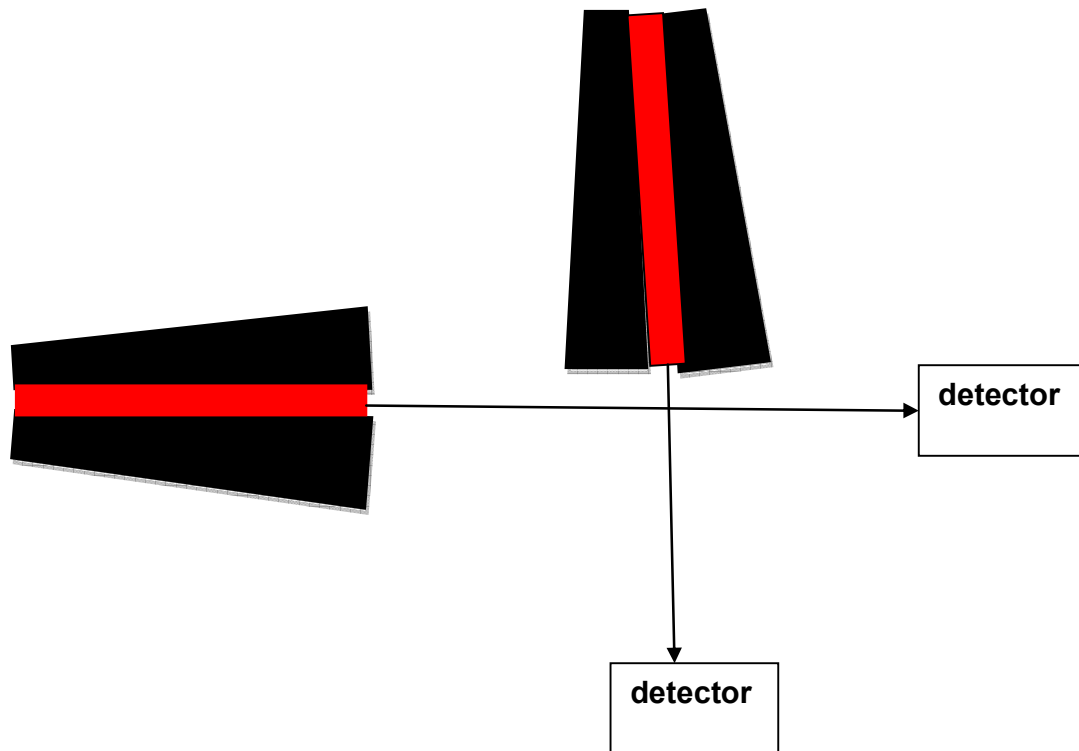


**Figure 26:** Configuration of two narrow  $\gamma$ -beams with extremely high intensity as possibly produced by conditions according to Figures 17, 19 and 23 to measure Heisenberg-Euler scatter.

## 5 References

- Abramowitz M, Stegun I 1970 *Handbook of Mathematical Functions with Formulas, Graphs and Mathematical Tables* National Bureau of Standards
- Aerts P J, Nieuwpoort W C 1985 *Chem. Phys. Letters* **113** 165
- Aerts P J 1986 *Chem. Phys. Letters* **125** 83
- 10 Bethe H A 1953 *Phys. Rev.* **89** 1256
- Euler H and Kockel B 1935 *Naturwissenschaften* **23** 1935
- Euler H 1936 *Ann. d. Physik.* **26** 398
- Eyges L 1948 *Phys. Rev.* **74** 1434
- Feynman R P 1962 *Quantum electrodynamics* (W A Benjamin Inc., New York)
- 15 Feynman R P and Hibbs A R 1965 *Quantum mechanics and path integrals* (Mac Graw Hill, New York)
- GEANT4-Documents 2005 <http://geant4.web.cern.ch/geant4/G4UsersDocuments/Overview/html/>
- Grant I P and Quiney H M 2002 *Theoretical and Computational Chemistry* **11** 107
- Heisenberg W and Euler H 1936 *Z. Physik* **98** 714
- Molière G 1955 *Z. Naturforschung* **10a** 177

- Quiney H M, Grant I P, Wilson S 1989 *J. Phys. B* **22** L15
- Saitoh S 2004 *Appl. Analysis* **83** 727
- Salvat F, Martinez J D, Mayol R, Parellada J 1987 *Phys. Rev. A* **36** 467
- Svensson R and Brahme A 1996 *Phys. Med. Biol.* **41** 1353
- 5 Ulmer W and Matsinos E W 2010 *European Physics Journal (Special Topics)* **190** 1 DOI:10.1140 A preprint is available in <http://arXiv:1008.3645v1>
- Ulmer W, Pyyry J and Kaissl W 2005 *Phys. Med. Biol.* **50** 1767
- Ulmer W 2010 *Inverse Problems* **26** 085002
- Ulmer W 1983 *Int. J. Quantum Chem.* **23** 1931
- 10 Ulmer W 1980 *Theor. Chim. Acta* **55** 179
- Visser O, Visscher L, Aerts P J, Nieuwpoort W C 1992 *Theor. Chim. Acta* **81** 405